Chapter 4

Tumor homing dextran derived amphiphilic self-assembling polymer nanoarchitectures for stimuli responsive drug delivery

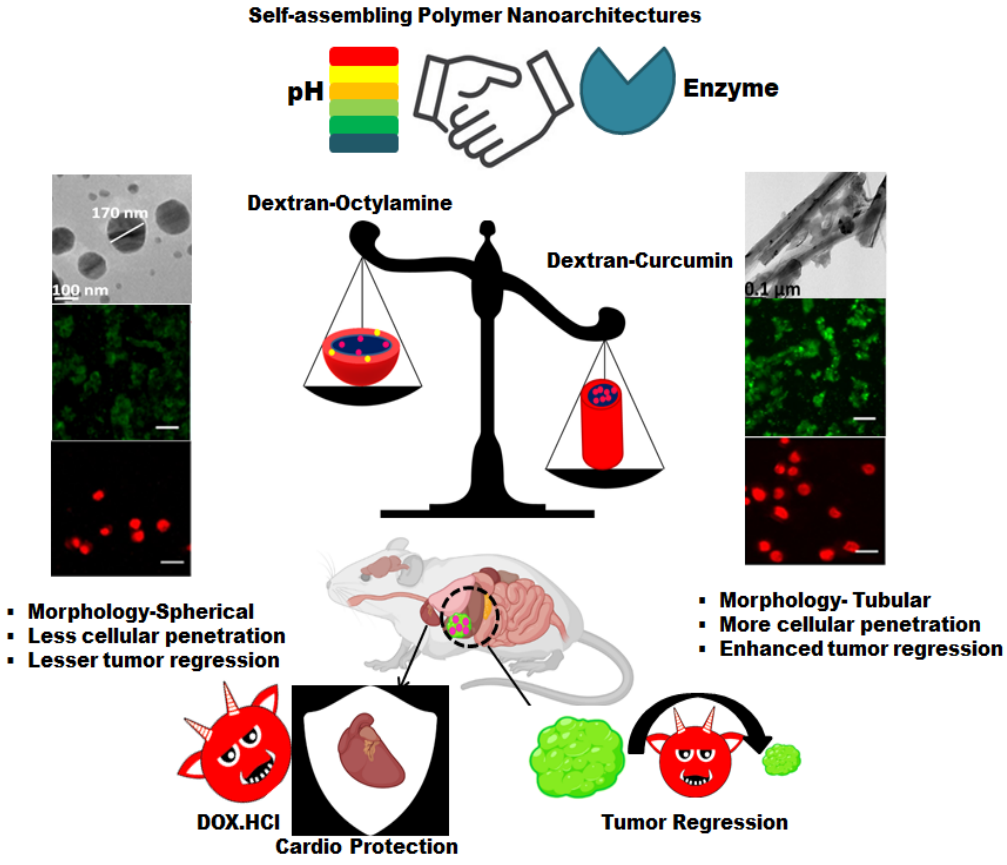

4.1 Introduction

The pharmaceutical industries associated with designing new drug molecules for cancer treatment are constantly facing the issue of poor therapeutic performance [1]. Even after investing huge amount of time (nearly 20 years) and capital (approximated cost of 500 million USD) for development of new drug molecules the issues of poor drug solubility, bioavailability and adverse side effects still remain a matter of concern to researchers. For instance doxorubicin hydrochloride (DOX.HCl) is the most effective therapeutic date so far in the chemotherapy regimen. It is a topoisomerase II inhibitor and can intercalate with cellular DNA to cause its disruption and subsequently apoptosis [2]. However it is sometimes referred to as red devil as it is associated with acute cardiotoxicity and other major side effects. Hence the conventional chemotherapy is rendered with less efficiency.

Nanotechnology derived formulations for delivering DOX.HCl has emerged as a promising strategy to tame its acute toxicity and improvise its efficacy[3,4]. Various strategies have been employed in the past few years for enhancing the efficacy of drug delivery by employing metallic nanoparticles like silver[5–7], gold[8–10] and magnetic iron oxide [11–13]. Several drug delivery vehicles have been designed using silica nanoparticles [14–16] carbon derived nanomaterials like carbon nanotubes [17–19] and grapheme [20–22] To further enhance their efficacy and to overcome other complications of the therapy like non-targeted nature of delivery and development of multiple drug resistance, such nanosystems were further evolved into multifunctional nanomaterials/nanoconjugates [23–27]. These multifunctional nanomaterials were engineered by an assortment of multiple functionalities like fluorescence, cancer cell targeting ligands, aptamers etc. to function as theranostic devices [28–32]. Despite of various advancements in the design of synthesis, such materials bear certain disadvantages like residual toxicity from the presence of metals in the carriers.

These challenges led the researchers towards the pursuit of developing biomaterial derived "smart polymeric nanocarriers". Owing to their wholesome non-toxicity, these bio-macromolecular carriers have emerged as much efficient drug carriers. This argument is supported by the fact that out of various nanomedicines approved by regulatory bodies for cancer

management, approximately 40% are either protein polymer conjugates or liposomes (Eg. Doxil, which is a liposomal formulation of Doxorubicin) [33,34]. Thus the development of such bio-macromolecular smart polymers with improvised efficacy and their effective clinical translation are the key steps in repositioning various anticancer drugs for more patient compliant treatment. Towards this goal, we have strategized the synthesis of stimuli responsive random amphiphilic polymers to tame doxorubicin (red devil) by controlled and targeted delivery. Amphiphilic polymers with appropriate functionalities, tend to self-assemble into various nanosized morphologies [35]. Interestingly such architectures are promising candidates as drug carriers owing to their long term stability, enhanced drug loading and excellent permeability.

We have developed some multi-stimuli responsive nanoconjugates in the recent past, for an efficient delivery of dual drugs to combat multidrug resistance (MDR) in cancer patients. Carbohydrates like cyclodextrin and dextran bear the required functionalities and also provide biocompatible matrix required to design drug carriers. Herein we report the synthesis of dextran derived enzyme and pH responsive, amphiphilic copolymers which can self-assemble to vesicular nanoarchitectures. It was observed that by changing the hydrophobic component molecule attached to dextran, the morphology could be tuned from spherical to tubular, which also, had strong influence on the drug payload carried by the nanocarriers. Interestingly, the potent but poorly bioavailable anticancer agent curcumin (golden spice) was employed as the one of the hydrophobic unit to construct the nanoarchitecture for delivery of anti-cancer drug. Curcumin is also an efficient sensitizer towards MDR cancer cells. It enhances the therapeutic response of MDR cancer cells towards conventional chemotherapeutic drugs due to its capability to cause down regulation of two major pathways for suppression of P-gp expression [36,37]. Several characterization techniques were utilized to prove the structure and function of the nanocarriers. The “in-vitro” cell line studies and “in-vivo” efficacy of these nano-architectures for liver cancer management evaluated on mice model also supported the effect of morphological variation.

4.2 Experimental Section

4.2.1 Materials and Methods

Dextran (MW 6000), curcumin, hexamethylene diisocyanate (HMDI), octylamine (OA), Amino group protected (NH-Boc) glycine and acetone were purchased from Sigma Aldrich, India. The anticancer drug doxorubicin hydrochloride (DOX.HCl) and phosphate buffer saline tablets (for preparation of pH 7.4 buffer solution) were also purchased from Sigma Aldrich. Disodium hydrogen phosphate, potassium dihydrogen phosphate, calcium chloride, potassium chloride, sodium hydroxide for preparation of PBS buffer pH 7.2 and 6.8 was received from Sisco Research Laboratories (SRL), India. Other reagents were of analytical grade, purchased from commercial sources and used as received without further purification. The solutions were prepared using de-ionized water.

FTIR spectra were recorded on a Bruker Alpha IR spectrophotometer at room temperature in the range of 4000-400 cm^{-1}. ^{1}H NMR and ^{13}C spectra was recorded on Bruker Avance 400 MHz spectrometer using tetramethylsilane as an internal standard and $CDCl_3$ or DMSO as solvents. High Resolution Transmission Electron Microscopy (HR-TEM) was recorded on Joel (Jem-2100F) electron microscope at 200 kV. For TEM analysis, the vesicles solutions were diluted at ambient temperature and dispersed on a carbon coated copper grid. The grids were air dried under ambient temperature environment overnight. Imaging was recorded using Jeol (Jem-2100F) electron microscope at 200 kV. Dynamic light scattering (DLS) was used to determine the hydrodynamic diameter and polydispersity of vesicles in the solution which was performed on Beckman Coulter Delso Nano. AFM and FESEM were recorded on NTEGRA PRIMA, NT-MDT, Russia and JSM7600F respectively. The fluorescence images were captured on a Nikon TI2E live imaging microscope. UV-vis spectrophotometric determinations were done using Perkin Elmer Lambda 35 and Fluorescence spectra were scanned on JASCO FP-6300.

4.2.2 Synthesis of DEXTRAN-Curcumin amphiphile

Step-1 DEXTRAN-CUR co-polymer formation via isocyanate functionalization: Mono o-acetyl curcumin was synthesized as per a previously reported procedure[38]. Mono o-acetylcurcumin 500 mg (3.8 mmol) was dissolved in 10 ml of DMSO purged with dry nitrogen. To this solution 300 μL of HMDI was added. The reaction was allowed to proceed for 1 h under ambient conditions (27°C) for 1 h. To this reaction mass, 500 mg (3.1 mmol of anhydroglucose

unit) of dextran dissolved in 5 ml of DMSO was added. The reaction was further allowed to proceed for 3 h at 27°C. The viscous reaction mass was precipitated using acetone (20 ml) to obtain yellow solid. The product was purified via precipitation process by dissolving the product in again in DMSO and re-precipitation with acetone. The yellow solid was given several washings of acetone, filtered and dried under vacuum at 60 °C. Yield: 1.0 g

Step-3 Synthesis of enzyme responsive DEXTRAN-OA copolymer (Dex-OA_{ER}):

Anhydrous DMSO (15 mL) was used to dissolve Dextran-curcumin (1 g) and NH-BOC Glycine (1g). This solution was purged then with nitrogen. DMAP (0.1 g) dissolved in 2 mL of anhydrous DMSO and DCC (1 g,) dissolved in 5 mL of anhydrous DMSO was then added to the above mixture. The reaction mixture was kept for stirring at 27 °C for 24 h. After 24 h, reduced pressure filtration was done for removal of remove dicyclohexyl urea; the process yielded a thick viscous liquid. Product was isolated by precipitation using 100 ----- of acetone. The solid was filtered and washed several times with acetone. It was re-dissolved in DMSO and purified via the precipitation technique twice. The product filtered and dried at 60 °C under vacuum to obtain yellowish white colored solid product. The final weight of the product was 1.75 g.

This polymer was designated as Dex-CUR_{ER} and explored further for vesicle formation and for enzyme responsiveness.

^{1}H NMR (400 MHz, DMSO-d6) δ ppm: 4.41, 4.82, 4.88 (s, hydroxyl of dextran), 4.64 ppm (s, dextran anomeric proton), 3.14−3.69 ppm (dextran glycosidic protons), 7.2 ppm (urethane linkage), 1.04-2.08 (repetitive unit of hexamethylene diisocyanate -CH_2), 6.7, 6.8, 7.2, 7.5 (characteristic protons of curcumin), 3.9 (-OCH_3, 6H, curcumin), 1.08 (H of Boc).

^{13}C NMR (400 MHz, DMSO-d6) δ ppm: 160.83 (C=O urethane), 98.10 (dextran anomeric carbon, 79.09 & 29.9 (C=O of Boc), 55.9 (-OCH_3 of curcumin), 183.4 (C-O, of curcumin), 121.3, 123.3, 126.5 (C=C & C=O, of curcumin), 79.13 & 29.92 (C=O of Boc) (Figure S6)

FTIR KBr (cm^{-1}): 3330, 1757, 1648, 1583

Step-3: De-protection of DEXTRAN-Curcumin-NH-BOC Glycine

TFA 0.39 mL was added **to** 0.5 g DEXTRAN-curcumin-NH-BOC Glycine dissolved in 4 mL of DMSO and kept under stirring for 4 h. On completion of 4 h, TFA was removed using a rota-evaporator and polymer purification was carried out by dialysis method. The polymer was

dialyzed against distilled water in a dialysis membrane of 3500 MWCO for 24 h. The dialysate was then lyophilized to get yellowish brown colored powder. The final weight of the product was 0.35 g.

This polymer was designated as Dex-CUR_{PR} and explored for pH responsiveness.

4.2.3 Synthesis of Dextran-Octylamine amphiphile

Step-1 DEXTRAN-OA co-polymer formation via isocyanate functionalization of OA: HMDI (300 µL) was added to a solution of 500 mg (3.8 mM) of OA dissolved in 10 ml of DMSO purged with dry nitrogen. The reaction was allowed to proceed for 1 hour at 27 °C. To this reaction mass, 0.5 g (3.1 mmol of anhydroglucose unit) dextran dissolved in 5 mL of DMSO was added. The reaction was further allowed to proceed for 3 h at 27°C. The viscous liquid was precipitated using acetone (30 ml) to obtain white solid. The product was purified via precipitation process by dissolving the product in again in DMSO and re-precipitation with acetone. The white solid was given several washings of acetone, filtered and dried under vacuum at 60 °C. The final weight of the product was 1.1 g.

Step-2 Synthesis of enzyme responsive DEXTRAN-OA copolymer (Dex-OA_{ER}):

Anhydrous DMSO (15 mL) was used to dissolve Dextran-OA (1 g) and NH-BOC Glycine (1g). This solution was purged then with nitrogen. DMAP (0.1 g) dissolved in 2 mL of anhydrous DMSO and DCC (1 g,) dissolved in 5 mL of anhydrous DMSO was then added to the above mixture. The reaction mixture was kept for stirring at 27 °C for 24 h. After 24 h, reduced pressure filtration was done for removal of remove dicyclohexyl urea; the process yielded a thick viscous liquid. Product was isolated by precipitation using 100 mL of acetone. The solid was filtered and washed several times with acetone. It was re-dissolved in DMSO and purified via the precipitation technique twice. The product filtered and dried at 60 °C under vacuum to obtain white colored solid product. The final weight of the product was 1.9 g. This polymer was designated as Dex-OA_{ER} and explored further for vesicle formation and for enzyme responsiveness.

^{1}H NMR (400 MHz, DMSO-d6) δ (ppm): 4.47, 4.82, 4.88 (s, hydroxyl of dextran), 4.63 (s, dextran anomeric proton), 3.14−3.69 (dextran glycosidic protons), 7.1 (urethane linkage), 1.04-

2.08 (repetitive unit of hexamethylene diisocyanate -CH_2), 2.6 ppm -CH_2 protons of OA, 1.08 (H of Boc).

^{13}C (400 MHz, DMSO-d6) δ (ppm): 160.8 (C=O urethane), 79.1& 29.9 (C=O of Boc), 98.10 (dextran anomeric carbon) (Figure S6)

FTIR KBr (cm^{-1}): 3335, 1756, 1650, 1581

Step-3: Synthesis of pH responsive Dex-OA_{PR} via de-protection of Dex-OA_{ER} 0.5 g DEXTRAN-OA-NH-BOC Glycine was dissolved in 10 mL of dried DMSO to which 0.39 mL of TFA was added and stirred for 4 h. After removing TFA on a rota-evaporator, the polymer was further purified by dialyzing against distilled water using dialysis membrane (MWCO 1.0 kDa) for 24 h, and then sample was lyophilized to get 0.09 g of brownish colored powder.

This polymer was designated as Dex-OA_{PR} and explored further for pH responsiveness.

1H NMR (400 MHz, DMSO-d6) δ (ppm): 4.47, 4.82, 4.88 (s, hydroxyl of dextran), 4.63 (s, dextran anomeric proton), 3.14−3.69 (dextran glycosidic protons), 7.1 (urethane linkage), 1.04-2.08 (repetitive unit of Hexamethylene diisocyanate -CH_2), 2.6 -CH_2 protons of OA. The peak at 1.08 ppm corresponding to protons of Boc group disappear post de-protection.

^{13}C (400 MHz, DMSO-d6) δ (ppm): 160.79 (C=O urethane), 98.12 (dextran anomeric carbon. The peak corresponding to the carbonyl carbon of Boc group disappear post de-protection (Figure S1 (A)).

4.2.4 Assessment of self-assembly of the amphiphilic polymer

For assessment of self-assembly, 0.1 wt% of the polymers were dissolved in DMSO and then subjected to extensive dialysis for removal of excess of DMSO before the following physical studies.

4.2.4.1 Vesicular assembly formation proved via FTIR studies

The solution of polymers were prepared in methanol as well as water and FTIR spectra was recorded by placing drops of polymer solutions between two CaF2 windows (path length = 0.2 mm). The spectra run were carried out with scan range of 4000−600 cm^{-1} with wavenumber precision of 0.005 cm^{-1}, number of scans recorded was 24 at 25 °C.

4.2.4.2 Dye encapsulation studies

The polymer solution (1 ml, 0.1 wt %) was internalized with calcein dye (30 μL, 1 X 10^{-3} mol L^{-1}) using DMSO solvent and diluted upto 3 mL using water. This solution was subjected to extensive dialysis against water (MWCO = 3500 Da) for 24 h for the removal of any un-encapsulated dye. The dialyzed solution was analyzed by UV-vis spectrophotometer showing peak at 484 nm that corresponds to λ_{max} of calcein. An emission spectrum was then recorded with this solution and compared to the absorption matched emission spectra of free dye in water.

4.2.4.3 Proof of concept of urethane linkage mediated self-assembly by Urea addition and DLS experiments for disassembly

These studies were carried out by spectroflourometric studies; 5 mg of solid urea was added to a calcein encapsulated polymer solution used for studies as per section 4.2.4.2. A complete dissolution of by stirring was ensured prior to spectral measurements. For DLS measurements 0.1 wt % of polymer solution was treated using 5 mg urea. The DLS spectra was recorded prior to and post the addition of urea.

4.2.5 Encapsulation of drugs in the nanoarchitectures

4.2.5.1 Loading the tubular systems (DEX-CUR_{ER} and DEX-CUR_{PR}) with DOX.HCl

The tubular nanocarriers were loaded with DOX.HCl via dialysis method. For the loading, polymer (5.0 mg) and DOX.HCl (0.5 mg) were mixed and dissolved in DMSO (2.0 mL). To this mixture 3 mL of double distilled water was added dropwise and kept under stirring in the dark for 4 h. Post this process, the mixture was transferred to a semipermeable dialysis membrane having MWCO 3500 Da. The dialysis was carried out against double distilled water for 48 h to ensure removal of the free drug and DMSO. During dialysis periodic replenishment of fresh water was ensured. The dialysate was filtered, lyophilized, and stored at 4 °C in dark. The drug loading content (DLC) and drug entrapment efficiencies (DLE) were determined by UV-visible spectrophotometry by recording the absorbance of DOX at 480 nm. The following equations 1&2 were used for quantification.

DLE (%) = [weight of drug in carrier/weight of drug in feed] X 100 --------- (1)

DLC (%) = [weight of drug in carrier/weight of carrier taken] X 100 --------- (2)

4.2.5.2 Loading the spherical systems (DEX-OA_{ER} and DEX-OA_{PR}) with DOX.HCl and curcumin

The spherical vesicles were co-loaded with both anticancer drug doxorubicin and anticancer agent curcumin via dialysis method. For loading, polymer (5 mg) and drug (0.5 mg: 0.25 mg DOX.HCl & 0.25 mg curcumin) were dissolved in DMSO (2.0 mL) and rest of the protocol is similar to tubular system loading. For calculation of DLC and DLE, absorbance of DOX was recorded at 480 nm and for Curcumin absorbance at 430 nm was measured.

4.2.6 In-Vitro Drug Release Studies for DOX.HCl and curcumin from nanocarriers

The in-vitro release profiles of DOX.HCl from DEX-CUR and both DOX.HCl as well as curcumin from DEX-OA was determined by dialysis method. Briefly 3.0 mg of the drug loaded nanocarriers were dispersed in 3 ml of PBS (pH = 7.4) and transferred to a dialysis bag with MWCO 3500 Da. The dialysis bag was immersed in 100 mL PBS 7.4 and maintained at 37 °C. At pre-decided time 3.0 mL of the media was withdrawn and replenished with equal volume of fresh media to maintain the concentration.

The absorbance of the solutions taken out was measured and amount drug was calculated by Beer's law. The same process was employed for studying drug release under PBS buffer pH 7.2 and 6.8. Similarly release study of DOX.HCl in FBS at 37 °C was also carried out to assess the release from carriers under physiological conditions.

For monitoring drug release under enzymatic conditions, similar protocol was followed by adding 10U of esterase enzyme in the dialysis bag (MWCO 1.0 KDa). The percentage cumulative drug release form nanocarriers were calculated using the equation 3.

$$\textbf{\textit{Cumulative drug release}} = \frac{\textit{Amount of drug released in time 't'}}{\textit{Total amount of drug in carrier taken in dialysis bag}} \times 100 \quad \textbf{-- (3)}$$

4.2.7 In-vitro studies

4.2.7.1 Cell culture and cell viability assay

These studies were performed on MCF-7 (Human breast cancer adenocarcinoma cell Line) was procured from National Centre of Cell Sciences, Pune, India. The cell lines were treated as per the protocols mentioned in the previous chapters for MTT assay.

4.2.7.2 Hemocompatibility of the carriers via hemolysis assay

The hemolysis assay was carried out as per previously mentioned protocol. The blood samples were placed in vacutainer tubes having ethylene diamine tetra-acetic acid (EDTA) coating and treated using higher concentration (500µg/mL) of both DEX-OA_{ER} and DEX-CUR_{ER}, based on the results of MTT Assay. Untreated sample showing 0% hemolysis acted as the negative control and sample given treatment with distilled water giving 100% hemolysis was the positive control.

4.2.7.3 Cell mortality assay

Cells were seeded in 12 well plates and incubated with the DOX loaded carriers for 24 h. The cells were then washed with PBS and later 50 µg/ml of Propidium iodide (PI) was added to the wells and incubated for 15 minutes at 37°C [11]. The cell death occurred due to treatment with drug loaded carriers was observed and photographed using Floyid cell imaging station (Life Technologies, USA) at 400X.

4.2.8 In-vivo studies

4.2.8.1 Hepatocellular carcinoma nude mice tumor model

Balbc mice 28-30 g, n= 42, male/female were procured from Zydus Research Center, Ahmedabad, India. The animal experimentation was carried out as per the ethical clearance granted by the Institutional Animal Committee (IAEC) and CPCSEA. The animals were housed under standard conditions of LD 12:12 with food and water ad libitium under the standard conditions. For the inoculation of hepatic tumor, the mice were injected intraperitoneally with (1×10^6) HEPG2 cells. The animals were divided into various treatment groups. The nanocarriers and drug loaded nanocarriers were dosed as injectable formulations intraperitoneally. The experiments were continued for 14 days. At the completion of stipulated experimental time period, body weights and weight of various organs were calculated. The blood samples were collected by puncturing the retro-orbital sinus and serum was separated by cold centrifuge at 3000 rpm. The liver functions were assessed by analysis of hepatic markers (SGPT and SGOT)

using standard kits (Reckon diagnostics Ltd., Vadodara, India). The matrix modulation markers (MMP-2 and 9) and serum marker of HCC i.e. AFP were also evaluated by ELISA kits (Krishgen Biosystems, Mumbai, India). After termination of the experiments, animals were sacrificed under mild ether anesthesia and liver autopsy was conducted.

4.2.9 Statistical analysis

All experiments have been performed at least in triplicate and expressed as means ± standard deviation (SD). The differences among groups were analyzed using the paired, two-sided Student's t-test. Values were expressed as mean ± SD of 4 animals. ANOVA was used to determine the statistical significance, using GRAPHPAD PRISM software. Significance in the figures are marked as * when compared with Control group and # when compared with Gep-G2 Induced group. *$p<0.05$, ** or ## $p<0.01$, ***$p<0.001$, **** or #### $p<0.0001$.

4.3 Result and Discussions

4.3.1 Designing of curcumin derived amphiphilic polymers and their self-assembly into various nanoarchitectures

Amphiphilic random co-polymers have the potential to self-assemble into aggregates of varying morphologies like micelles, vesicles, rods and hollow tubes. They possess the potential of exhibiting morphological transitions by appropriate tuning of hydrophilic to hydrophobic ratio (HLB), which is an interesting property to manoeuvre for drug delivery applications.

For the synthesis of amphiphilic random co-polymer, dextran was selected as the hydrophilic unit owing to its renewable nature and biocompatibility [39]. Another such biocompatible and medicinally important molecule, curcumin, was selected as the hydrophobic unit to be incorporated into the polymer skeleton (designated as DEX-CUR). The two components were linked together using urethane linkages.

For comparison another amphiphilic random co-polymer was synthesized with octylamine as the hydrophobic unit (designated as DEX-OA). Both these polymers were further adorned with amino acid glycine via labile amide linkages to render stimuli responsiveness to the carriers thus ensuring the release of drug cargo in a targeted fashion.

For the synthesis of DEX-CUR as per **scheme 4.1**, acetylcurcumin was first reacted with HMDI to prepare pre-polymer "A" with a reactive NCO as the end group. These free NCO groups then reacts with dextran by the formation of urethane linkages to obtain an amphiphilic polymer.

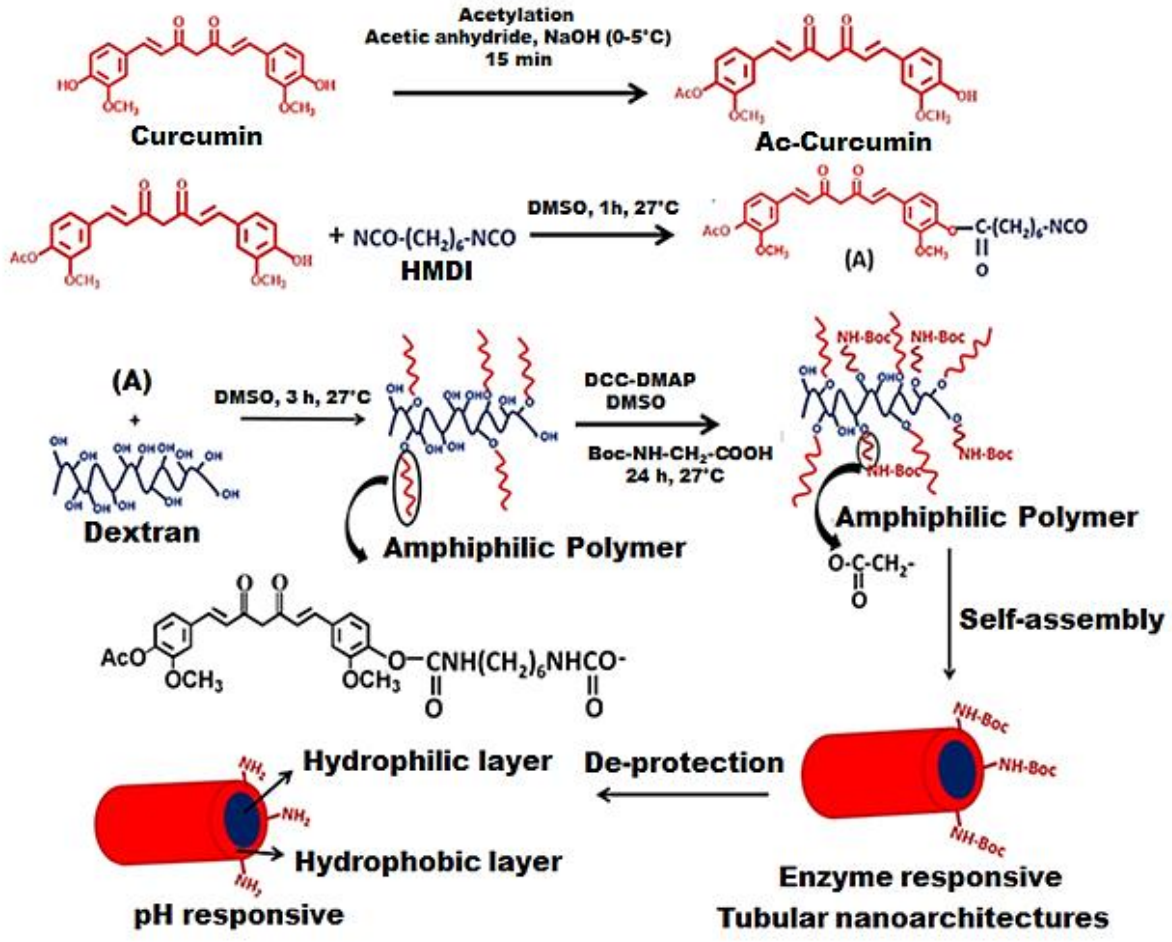

Scheme 4.1: Schematic for synthesis of pH and enzyme responsive DEX-CUR co-polymer and representation of their subsequent self-assembly into tubular nanoarchitectures

The utilization of HMDI fulfills two criteria in the synthetic strategy; Firstly, it acts as a linker for combining the hydrophilic and hydrophobic segments. Secondly, the introduction of urethane in the polymer backbone supports the intrachain H-bonding formation thus opening avenues for H-bonding mediated self-assembly [40].

The carboxyl functionalities of NH-Boc protected glycine was then reacted with the free hydroxyl groups of dextran in the polymer via esterification reaction.

The same synthetic strategy was employed for preparation of DEX-OA as shown in **scheme 4.2**.

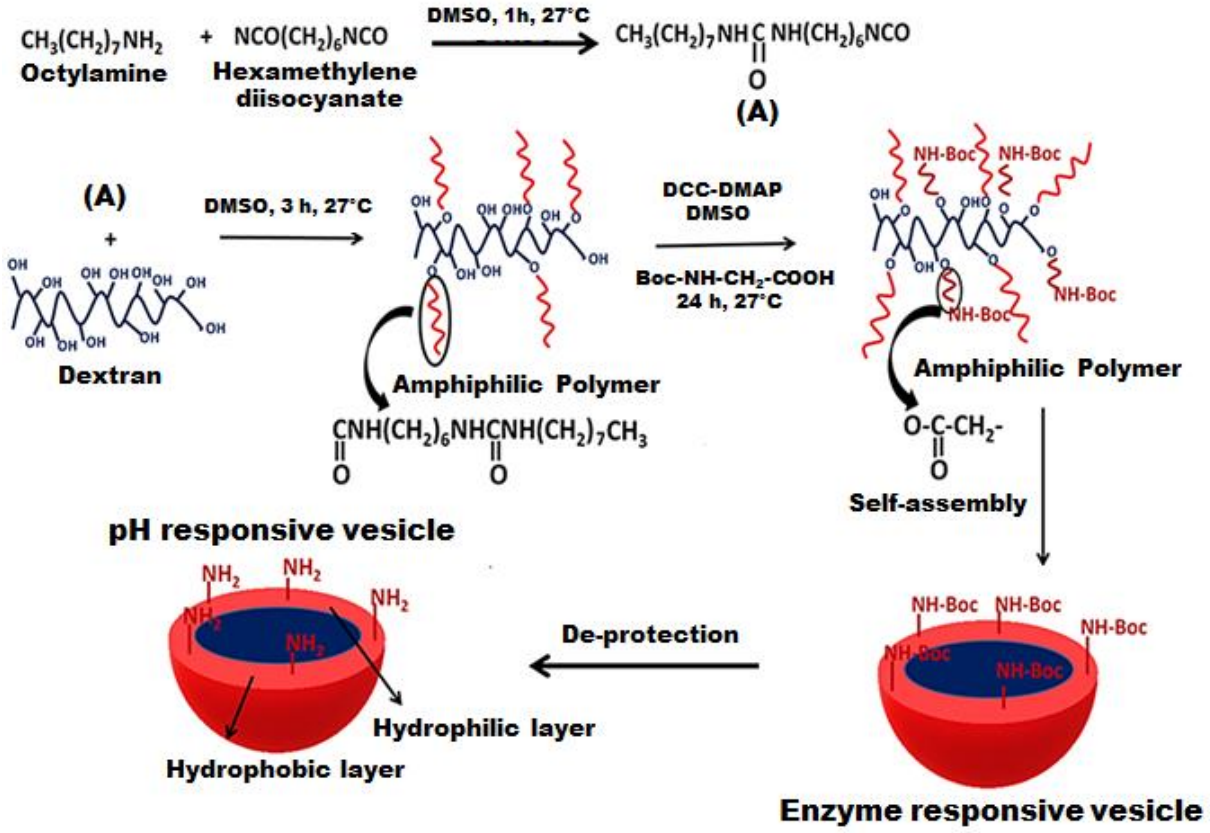

Scheme 4.2: Schematic for synthesis of pH and enzyme responsive Dex-OA co-polymer and representation of their subsequent self-assembly into vesicles

The amphiphilic polymers thus synthesized are expected to self-assemble into vesicular nanoarchitectures by virtue of H-bonding of urethane linkages. Upon endocytosis in the cancer cells, the amine of the drug-loaded nanocarriers is de-protected, due to enzymatic hydrolysis in the late endosomal compartments. The free amino groups render the nanocarriers pH responsive designated as DEX-CUR$_{PR}$ and DEX-OA$_{PR}$. The polymers were analyzed with NMR and FTIR for their structural evidence **(as shown in Figure 4.1, 4.2, 4.3 & 4.4).**

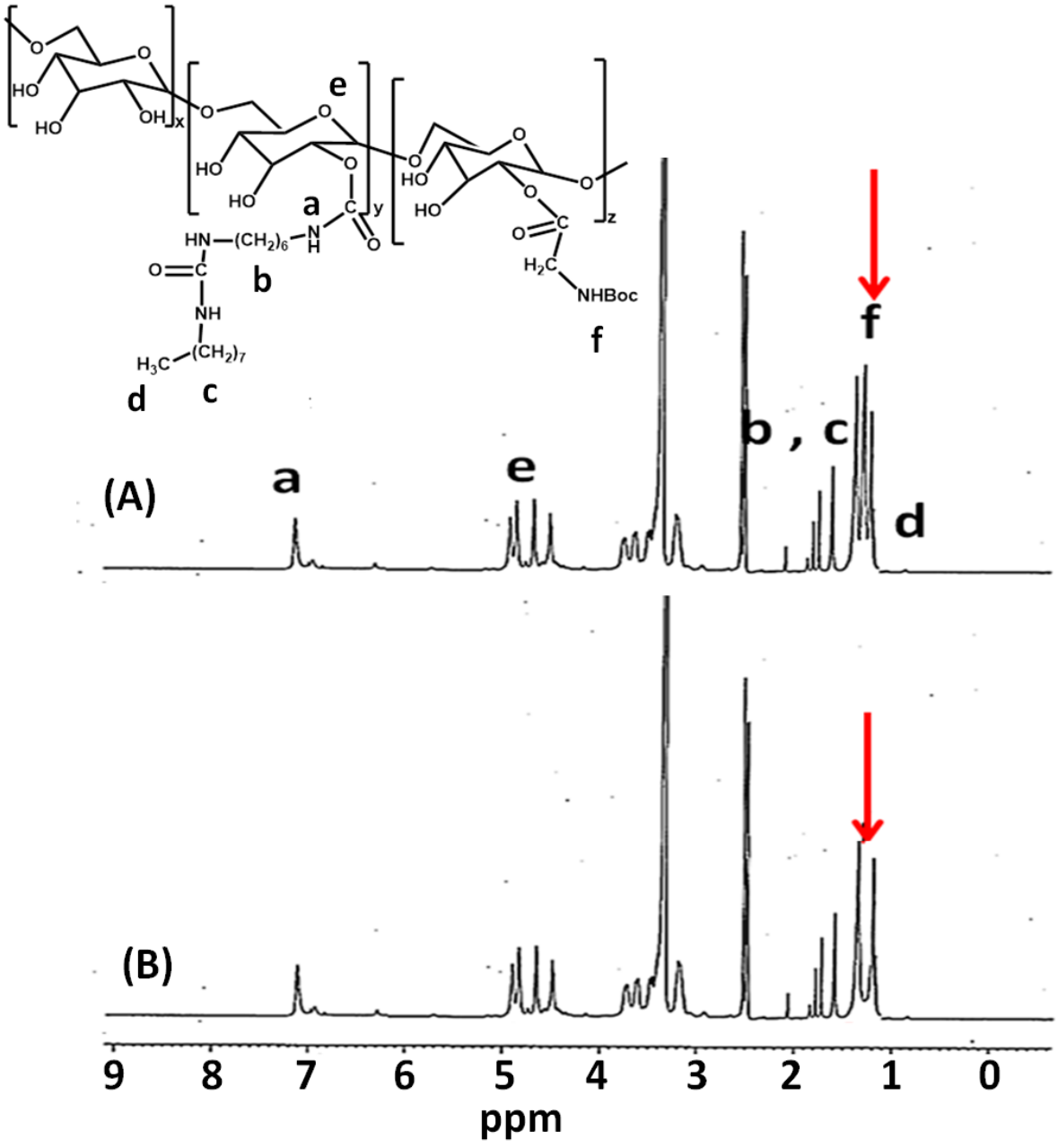

Figure 4.1: ^{1}H NMR spectra of octylamine unit containing dextran derived co-polymer (A) with and (B) without Boc protection

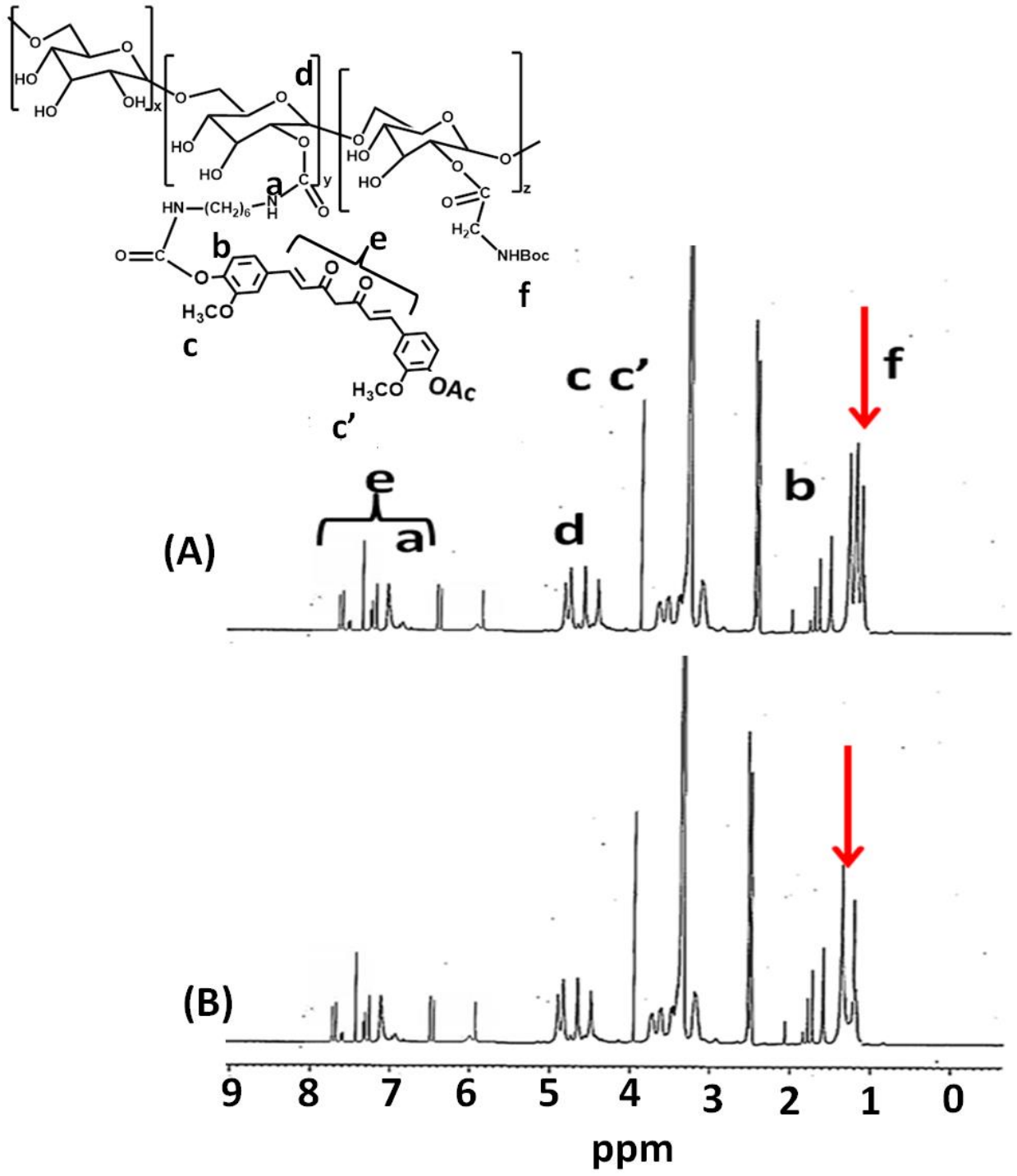

Figure 4.2: ^{1}H NMR spectra of curcumin unit containing dextran derived co-polymer (A) with and (B) without Boc protection

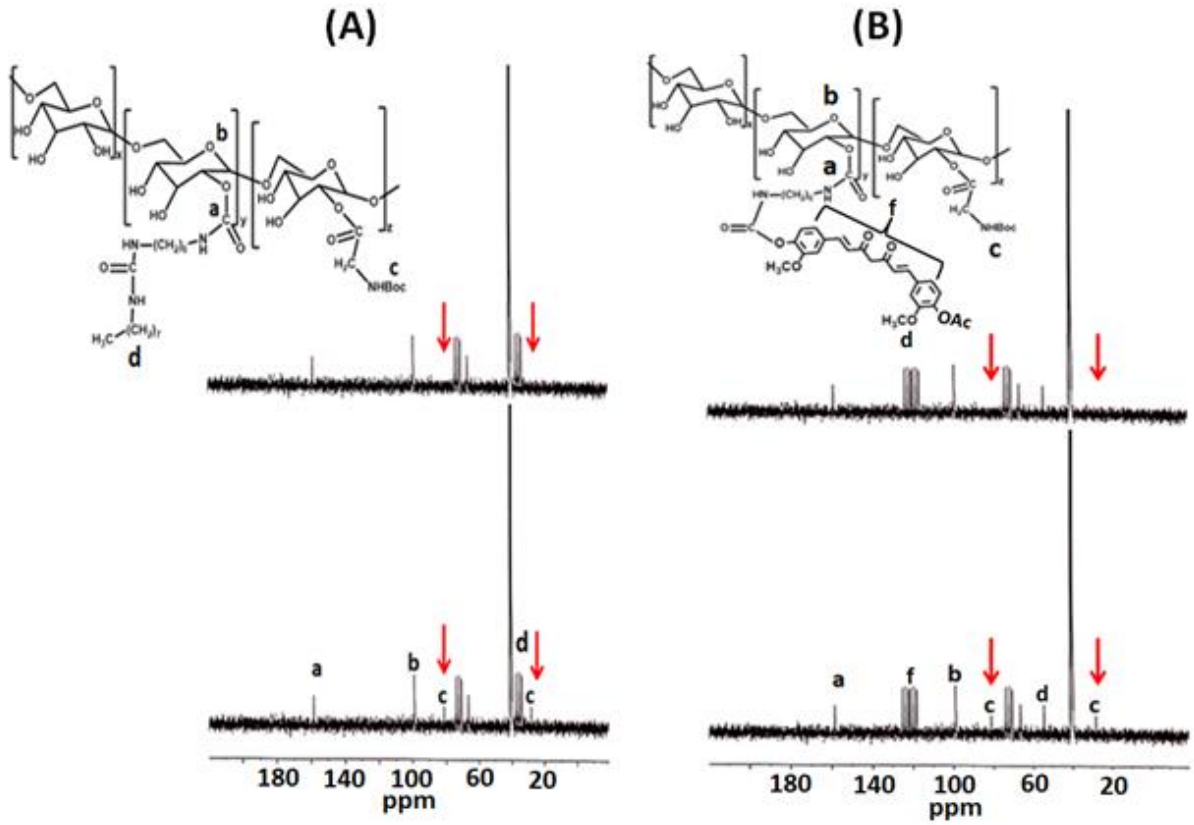

Figure 4.3: ^{13}C NMR spectra of (A) DEX-OA and (B) DEX-CUR polymers

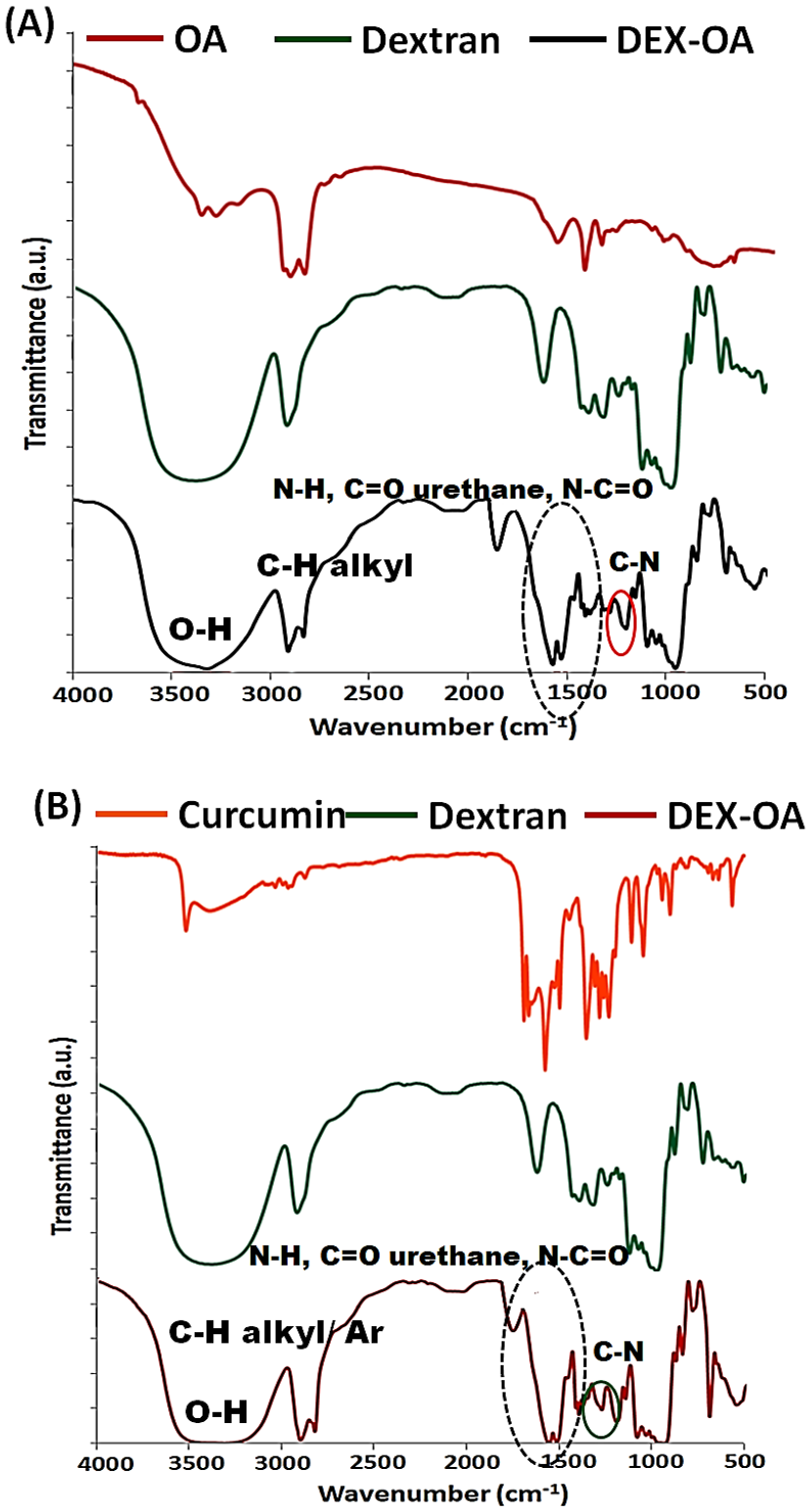

Figure 4.4: Overlay of FTIR spectra for (E) DEX-OA_{ER} and (F) DEX-CUR_{ER} polymers

In case of both DEX-OA_{ER} and DEX-CUR_{ER} the successful incorporation of urethane linkage containing octylamine/curcumin fragment on the dextran skeleton was confirmed due to the appearance of proton corresponding to urethane linkage around 7.0-7.5 ppm in addition to the signature peaks of dextran as shown in **figure 4.1A & 4.2A**. The aromatic protons corresponding to the presence of curcumin appear in the NMR spectra of DEX-CUR_{ER} **(figure 4.1)**. The ^{13}C NMR indicated the presence of carbonyl carbon of urethane linkage at 160-161 ppm further confirming the conjugation **(figure 4.3).** Further, the conjugation of NH-Boc-Glycine was confirmed from the presence of proton corresponding to its NH-Boc group at 1.08 ppm in ^{1}H spectra and the carbonyl carbon of Boc group appeared at 79.13 and 29.92 ppm in ^{13}C spectra for both the enzyme responsive polymers.

Upon de-protection of the Boc functionality, the polymers attain their pH responsive form DEX-OA_{PR} and DEX-$CUR_{PR,}$ these polymers were also subjected to characterization by NMR. It was observed that, all other characteristic peaks remain intact, only the peaks corresponding to the Boc group disappears from both ^{1}H NMR **(figure 4.1 B & 4.2B)** and ^{13}C spectra **(figure 4.3)**. The FTIR spectra shows the presence of characteristic peaks corresponding to free –OH groups of carbohydrate dextran, the carbonyl functionalities of urethane and ester linkages and aromatic stretching frequencies **(figure 4.4)**.

4.3.2 Analyzing the self-assembling phenomenon of the amphiphiles and drug loading capability

Before testing the potential of these amphiphilic polymers as drug delivery vehicles, they were subjected to 2 important assessments; (i) Assessing their capability to produce stable self-assembled nano-architectures and (ii) The ability of the nanoassemblies to encapsulate anticancer drugs.

For the first assessment, the theory of intrachain hydrogen bond mediated self-assembly into nanoassemblies was proposed and proved with the help of various studies. As stated earlier it is anticipated that urethane linkages in the polymer network drives the formation of these H-bonds **(figure 4.5 (i))**. The FT-IR spectrum of polymer was recorded both in methanol and water **(figure 4.5A)**. The carbonyl stretching frequency of urethane group appears at 1680 cm^{-1} in methanol and at 1641 cm^{-1} in water for both the polymers. The shift in the frequency value by 39

cm^{-1} confirms the presence of H-bonding in water. The nanoassemblies have distinct hydrophilic and hydrophobic regions; the self-assembled polymers have the capability to contain water molecules in its hydrophilic region. The formation of vesicular morphology was further proved by exploring the presence of this confined water pool by calcein encapsulation followed by fluorescence measurements [41]. The extensively dialyzed solution of the calcein encapsulated polymer showed characteristics emission peak of Calcein at its λmax 510 nm **(figure 4.5B)**, indicating the localization of calcein in the water pool of both **DEX-CUR** tubes and **DEX-OA** spheres.

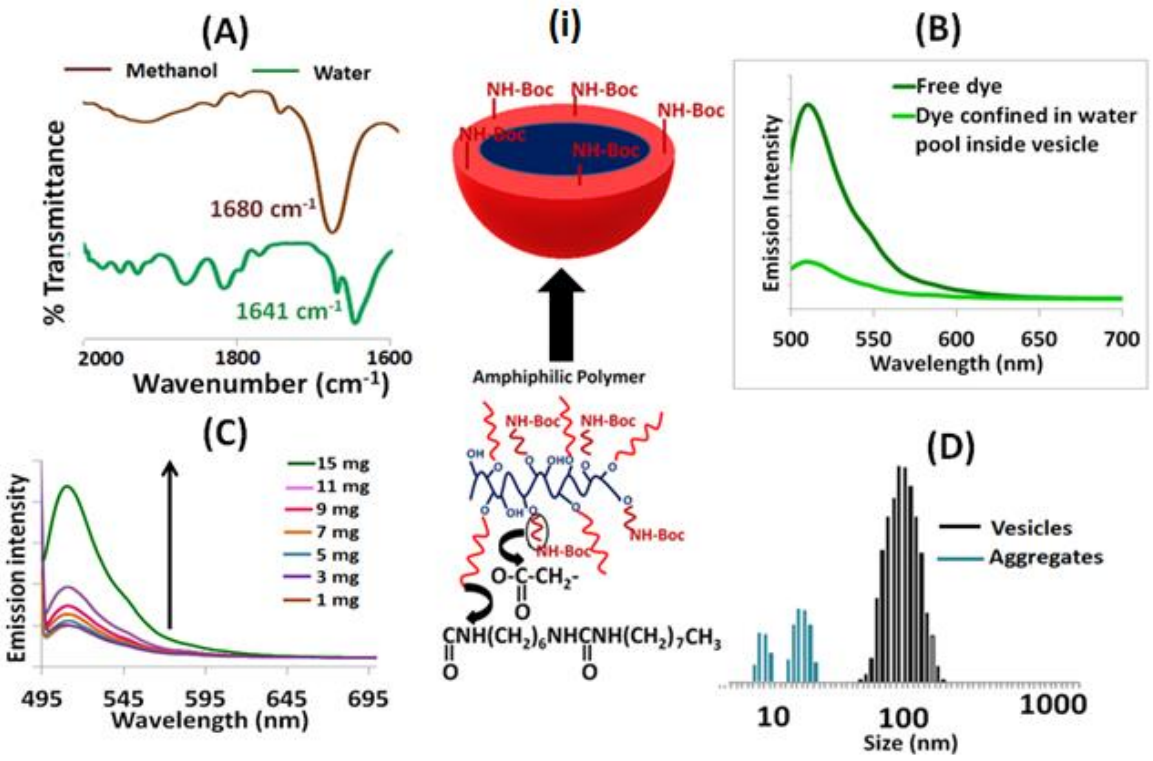

Figure 4.5: Proof of concept of self-assembly (as shown in (i)) via intrachain H-bonding of urethane linkages by various characterizations (A) FTIR spectra of DEX-OA_{ER} in methanol and water as recorded in CaF_2 window (B) self-quenching studies fluorescence measurement of free calcein and calcein encapsulated vesicle (C) urea addition experiments via fluorescence measurements (D) DLS spectra of the polymer showing size distribution before and after urea addition.

The emission intensity of calcein encapsulated polymer was compared to that of the absorption matched intensity of the free dye in water. A reduced emission intensity of calcein encapsulated in vesicles is an attribution of the phenomenon of self-quenching due to its confinement thus corroborating to the formation of vesicles.

This model is further proved with the means of urea addition experiments as urea has an affinity to disrupt the H-bonding [42]. The addition of urea to calcein loaded vesicular solution denatures the H-bonding and thus causing the vesicle to disassemble. Upon disassembly, there is a sudden expulsion of confined dye molecules in bulk water which is observed as an enhancement in emission intensity in fluorescence measurements **(figure 4.5C)**. The size distribution measurements align with this theory, the DLS spectrum of the polymer solution in absence of urea shows peak at 160 nm corresponding to presence of vesicles. On the contrary this peak completely disappears in the spectrum of the polymer solution with presence of added urea suggesting disassembly. Instead 2 new peaks are observed at 50 nm and 10 nm respectively which may be due to the formation of some undefined small sized aggregates post disassembly **(figure 4.5D)**. Moreover the dye encapsulated solution of these polymers was analyzed using fluorescence microscope and demonstrated bilayered green emitting spherical particles **(figure 4.6A & 4.6G)**. Thus it was confirmed that both DEX-CUR and DEX OA polymers can undergo self-assembly into nanoarchitectures (as shown schematically in **figure 4.6 i & ii**).

Later theses nanoarchitectures in their representative enzyme and pH responsive forms were loaded with drug. The drug entrapment and loading efficiencies of all the carriers DEX-$CUR_{ER,}$ DEX-CUR_{PR} DEX-$OA_{ER,}$ and DEX-OA_{PR} were assessed as shown in **table 4.1**. The DEX-OA nanocarriers were loaded with both hydrophilic anticancer drug DOX.HCl and hydrophobic anticancer agent curcumin. The DEX-CUR nanocarriers were loaded only with DOX.HCl. For making these formulations the polymer and drug were dissolved in a DMSO-water mixture and dialyzed against double distilled water in a dialysis bag for 48 h.

Table 4.1: Comparison of the drug entrapment efficiencies (DEE) and Drug loading capacities (DLC) of the synthesized nanocarriers

Carrier	Drug	DEE (%w/w)	DLC (%w/w)
DEX-CUR$_{ER}$	DOX.HCl	55	5.5
DEX-CUR$_{PR}$	DOX.HCl	53	5.2
DEX-OA$_{ER}$	DOX.HCl	50	5.1
	Curcumin	23	2.2
DEX-OA$_{PR}$	DOX.HCl	49	4.9
	Curcumin	25	2.6

The DEX-CUR nanocarriers were able to entrap more cargo of drug as compared to the DEX-OA nanocarriers. This observation suggests that topology of the nanocarriers had an influence on drug loading[43]. DEX-CUR carriers owing to their long tubular structure are able to hold more quantity of drug as compared to the spherical DEX-OA carriers.

4.3.3 Detailed analytical characterization of the bare and drug loaded nanoarchitectures

For further analytical characterizations all the dextran derived co-polymers were subjected to extensive dialysis using a semipermeable membrane against water. The morphological analysis of the solution of nanoarchitectures via FE-SEM imaging showed interesting observations. The presence of 175 nm sized spherical vesicles was noted for DEX-OA$_{ER}$ and ~1 μm long tubular structures were observed in case of DEX-CUR$_{ER}$ **(figure 4.6B & H)**. The morphology and size was further confirmed by HRTEM imaging. The DEX-OA$_{ER}$ system demonstrated the formation of spherical nanovesicles with formation of distinct bilayered structures **(figure 4.6C & D)**. The size was observed to be 170 nm with a peripheral thickness of 30 nm. However the DEX-CUR$_{ER}$ polymer solution showed the presence of tubular morphologies. The mouth of the tubes were found to be nearly hexagonal with size of around 15 nm and the tubes were found to be ~1 μm long **(figure 4.6 I & J)**. These observations are in agreement with some previous studies reported in the literature that state that amphiphilic random copolymers possess the ability to form various kinds of nanoarchitectures [35]. The structural aspects of these nanoarchitectures can show transition depending upon certain factors like solvent, monomer, nature of building blocks used synthesis of the co-polymer etc [44,45] .

In the present study it was observed that changing the hydrophobic monomer assisted the polymer to attain an altogether different nano architectural morphology. The size distribution observed in dynamic light scattering (DLS) measurement of the aqueous polymer solutions was similar to those observed form HR-TEM analysis with inset images showing the formation of stable clear polymer solutions **(figure 4.6E & K)**. Both DEX-OA_{ER} and DEX-CUR_{ER} showed mono-model distribution, good autocorrelation and sizes <250 nm (figure 4E & 3K). Since it is hypothesized that, the enzyme cleavage will occur at the NH-Boc linkages of the self- assembled amphiphilic polymer. Control experiments were performed by subjecting DEX-OA_{ER} and DEX-CUR_{ER} to 10U of esterase enzyme at 37°C for 48 h. The DLS data did not show any appreciable alteration in the size of self-assembled nanostructures for both the polymers **(figure 4.7)**. This confirms the cleavage of the polymers at the desired functionality.

AFM was further used to probe the morphological details of the polymers. DEX-OA_{ER} demonstrated spherical shaped vesicular objects with an average size of 145 nm whereas, DEX-CUR_{ER} were tubular structures having an average size of 1-1.5 μm **(figure 4.6 F & 4L)**. A smaller height as compared to the width in height profiling further proved the vesicular morphology.

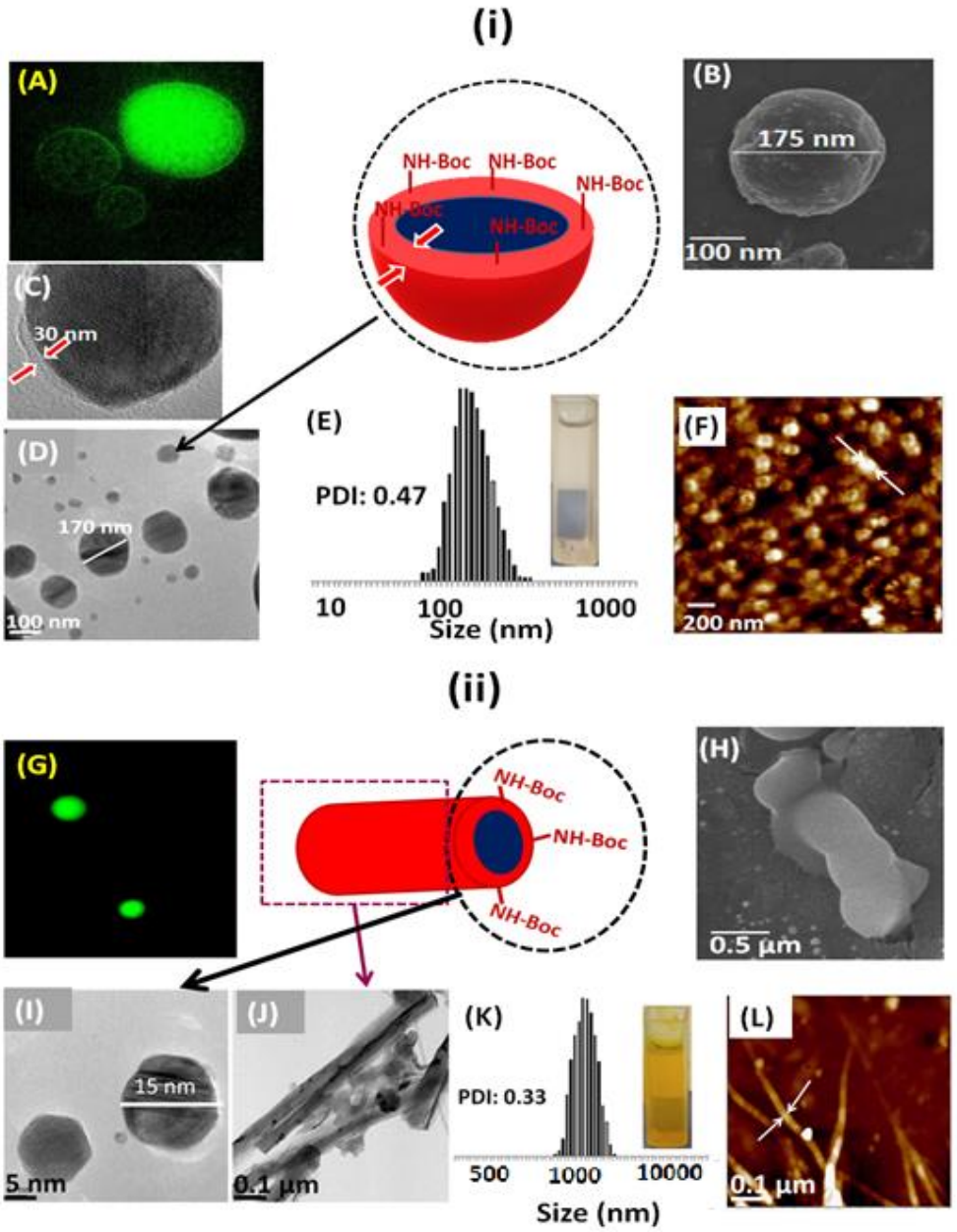

Figure 4.6: (i) characterization of DEX-OA$_{ER}$ (A) fluorescence microscopic (B) FE-SEM (C) & (D) HR-TEM images (E) DLS histogram with (inset: digital image of a vial containing the vesicular solution and (F) AFM image; (ii) characterization of DEX-CUR$_{ER}$ (G) fluorescence microscopic (H) FE-SEM (I) & (J) HR-TEM images (K) DLS histogram with (inset: digital image of a vial containing the vesicular solution) and (L) AFM image. (The samples were maintained at 0.1 mg/ml for DLS and 0.05 mg/ml for rest of the imaging)

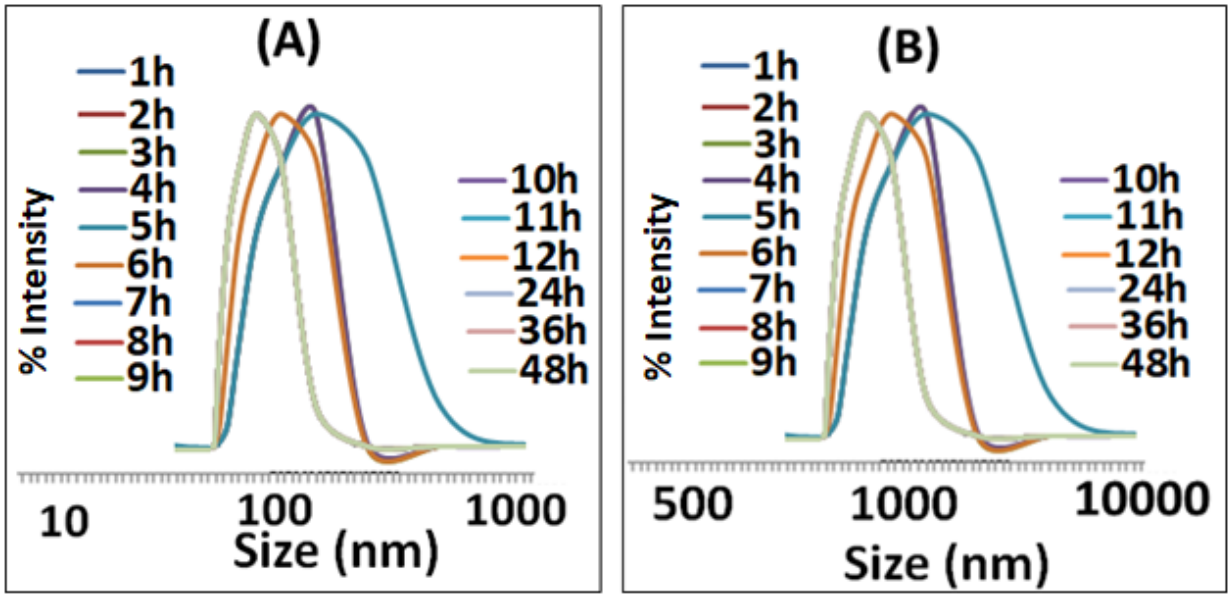

Figure 4.7: DLS plots showing size distribution of (A) DEX-OA_{ER} and (B) DEX-CUR_{ER} in the presence of esterase enzyme at 37 °C for 48 h.

The drug loaded polymer samples were also subjected to HRTEM, DLS, FESEM and AFM analysis. An increase in size was observed for the nanoarchitectures post drug loading however there was no change in their geometries in all the analytical measurements as shown in **figure 4.8 & 4.9**. DEX-OA_{ER} showed an increase in size by 20 nm as a result of drug entrapment **(figure 4.8 B)**. The mouth of DEX-CUR_{ER} tubes also widened from 15 nm to 22 nm because of drug loading **(figure 4.9 B)**.

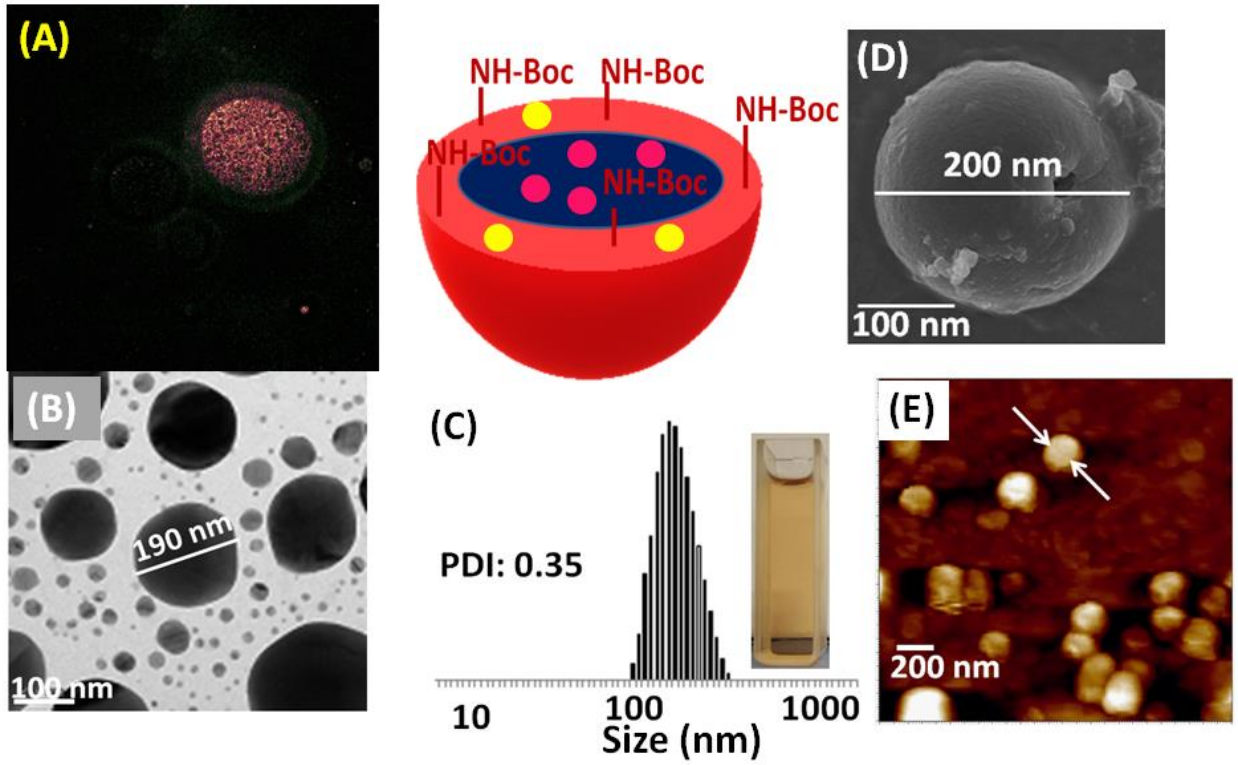

Figure 4.8: (A) Fluorescence microscopic (B) HR-TEM (C) DLS histogram (inset: digital image of a vial containing formulation of drug loaded vesicles) (D) FE-SEM (E) AFM images of curcumin and DOX.HCl co-loaded DEX-OA_{ER}. (The samples were maintained at 0.1 mg/ml for DLS and 0.05 mg/ml for rest of the imaging)

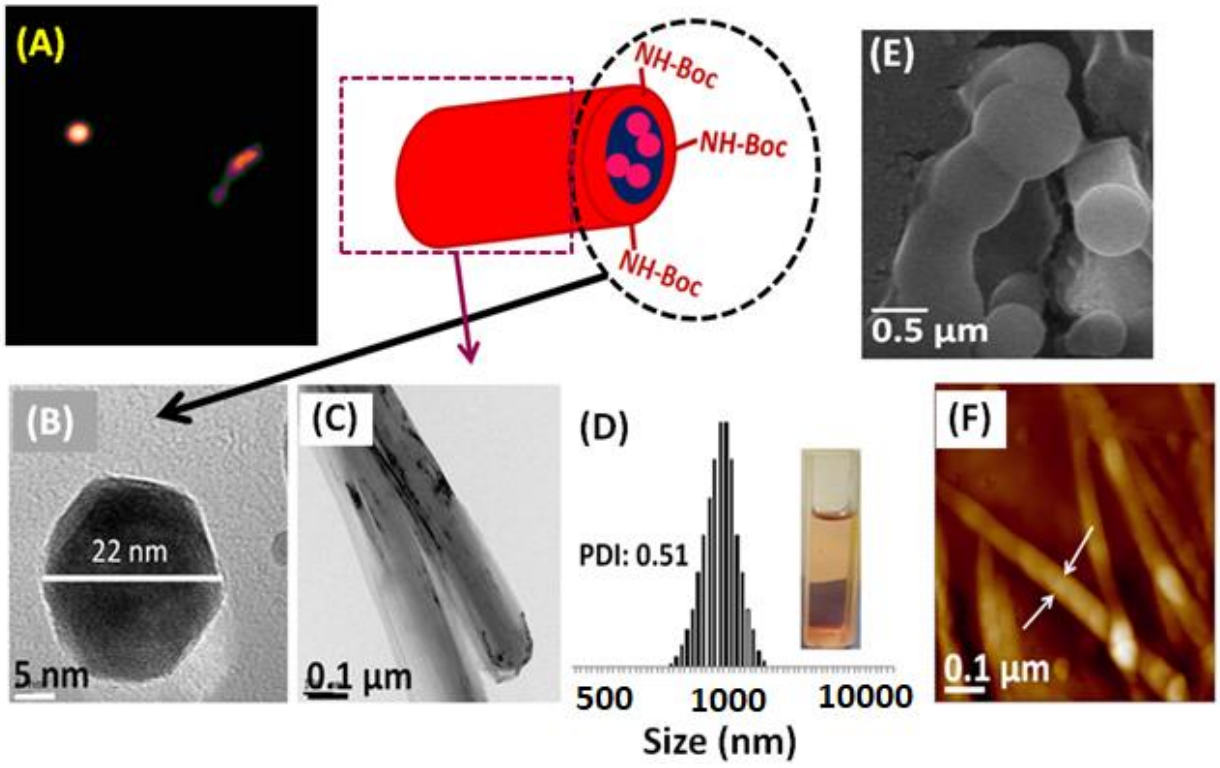

Figure 4.9: (A) Fluorescence microscopic (B) & (C) HR-TEM (D) DLS histogram (inset: digital image of a vial containing formulation of drug loaded vesicles) (E) FE-SEM (F) AFM images of DOX.HCl loaded CUR-OA_{ER}. (The samples were maintained at 0.1 mg/ml for DLS and 0.05 mg/ml for rest of the imaging)

4.3.4 In-vitro drug release from nanoarchitectures under conditions of mimicked tumor microenvironment (enzyme and pH responsive release)

DEX-CUR_{ER} and DEX-OA_{ER} are susceptible to undergo biodegradation in the enzyme rich late endosomal compartment as represented in **figure 4.10A**. Thus they were subjected to enzymatic conditions mimicked by using 10U of esterase at 37 °C in pH 7.4. For comparison the in vitro release was also observed in absence of esterase. The % cumulative release profiles obtained from these experiments under various conditions are shown in **figure 4.10B & 4.10C**. The release profile in **figure 4.10B** revealed excellent stability of the nanoarchitectures under physiological conditions (PBS saline) with only 25% leaching of both DOX.HCl and curcumin from DEX-OA_{ER}. When vesicles are subjected to treatment of esterase enzyme, they are ruptured to release 70% curcumin and 80% DOX.HCl from DEX-OA_{ER} vesicles.

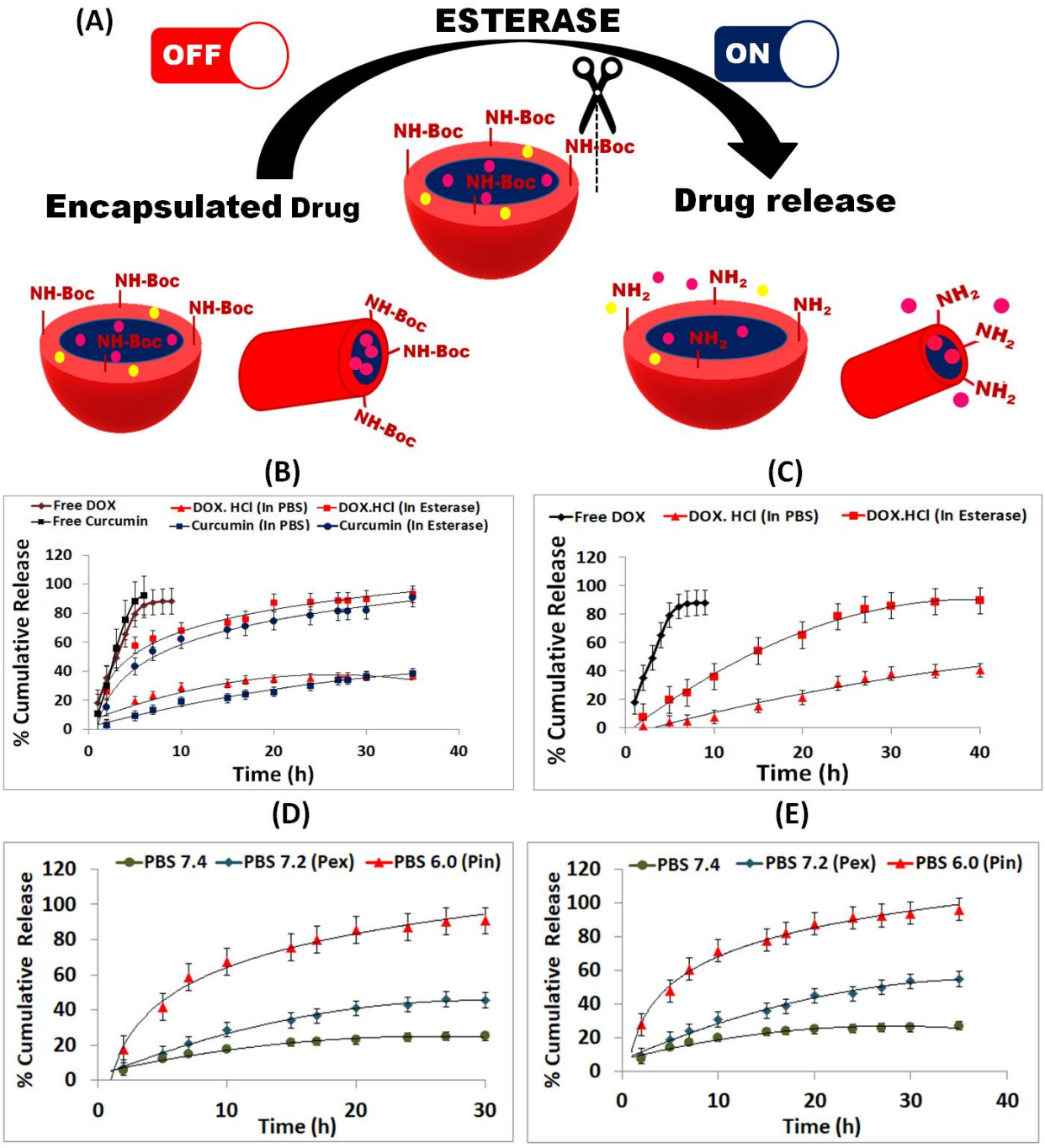

Figure 4.10 (A) Schematic representation of enzyme responsive transition in the carriers (B) cumulative release of DOX.HCl and curcumin from DEX-OA_{ER} and (C) DOX.HCl from DEX-CUR_{ER}, pH responsive DOX.HCl release from (D) DEX-OA_{PR} and (E) DEX-CUR_{PR}

Similar release profile was obtained from DEX-CUR_{ER} with less than 30% DOX.HCl release in absence of esterase and more than 85% in presence of esterase **(figure 4.10C)**. This is an indication that the drug release post enzymatic cleavage from both vesicles and tubes follows similar kinetics [43].

The advances in detailed study of cancer cells reveal the existence of a differential pH between blood vessels (pH 7.4), extracellular (pH 6.5-7.2) and intracellular (pH 5.0-6.0) void in tumor [46]. This differential pH plays a major role in various functions of the cell and assists in development of cancer and its treatment [47]. The existence of this differential pH can be exploited to design carriers that are sensitive to pH for high therapeutic efficacy [48]. Such carriers should also be able to undergo some physical or chemical changes like charge or size transition for unloading the drug in response to pH at the tumor site.

With this background, the drug loaded DEX-OA_{PR} and DEX-CUR_{PR} were subjected to 3 varying pH conditions. PBS buffer 7.4 was selected as the physiological pH, whereas PBS buffer 7.2 was used to mimic extracellular pH and PBS buffer 6.0 as intracellular pH of cancer cells. The cumulative release profiles in figure 4 demonstrated less than 30% leaching at pH 7.4 from both spherical vesicles and tubes which is indicative of low toxicity normal cells. Under the mimicked extracellular pH (7.2) conditions, ~ 60% of DOX.HCl **(figure 4.10D)** and ~50% of curcumin **(figure 4.11)** is released from spheres. Similarly in case of tubustecan carriers ~55% of DOX.HCl release was observed at pH 7.2 **(figure 4.10E)**. A further drop in the pH to 6.0 causes the cationic polymer to swell and thus expelling more than 90 % the entrapped DOX.HCl molecules in the tumor microenvironment from both the carriers. In case of spherical vesicles also ~80% of curcumin is released at pH 6.0 **(figure 4.11)**.

The spheres demonstrated a 30h sustained release whereas tubes had the capability to release upto 35h. This can be attributed to the tubular shape of the carriers that hold more cargo of DOX.HCl. Moreover the small mouth aperture of the tube assist in a slow and sustained release hence few more hours are required to unload maximum amount of drug.

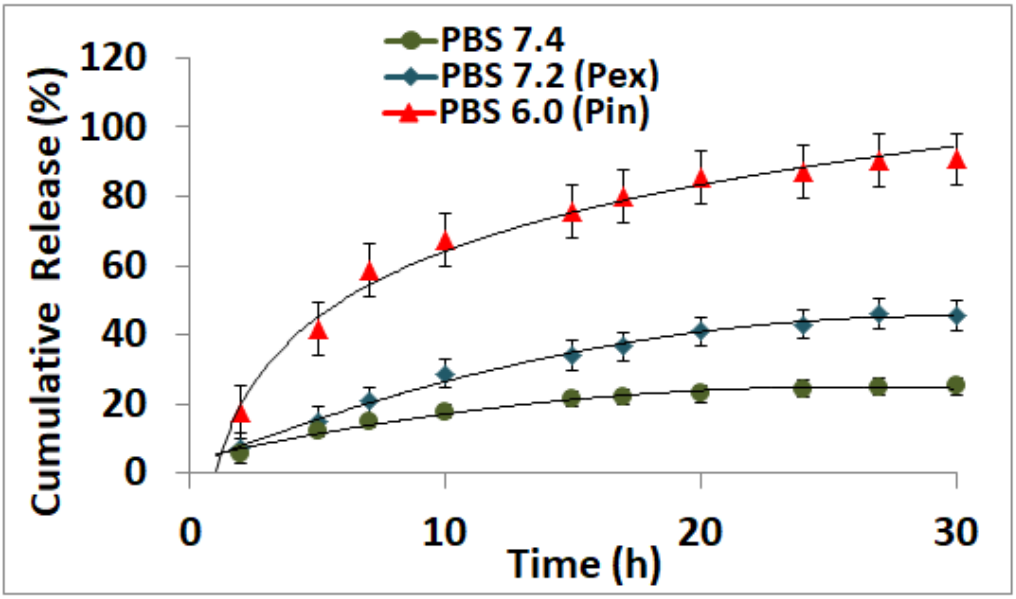

Figure 4.11: Cumulative release profile of curcumin from DEX-OA_{PR}

These findings are in concurrence with literature findings which suggests that the shape of nanoarchitectures has an enormous role in the cellular internalization and accumulation in the tumor [49]. This is due to the influence in the phagocytic or endocytic carrier uptake due to variation in the shape of the carrier [50].

Further, in order to evaluate the stability of these carriers in blood plasma, both DOX.HCl loaded DEX-OA_{ER} and DEX-CUR_{ER} were incubated in FBS at 37 °C and the release profiles were studied **(figure 4.12)**. The release profiles suggested that both the systems were stable against the proteins present in FBS with only <30% drug leaching. This suggests that more that 70% of the drug remains available that is susceptible to release exclusively upon lysosomal degradation by esterase within the cytoplasm of cancer cells.

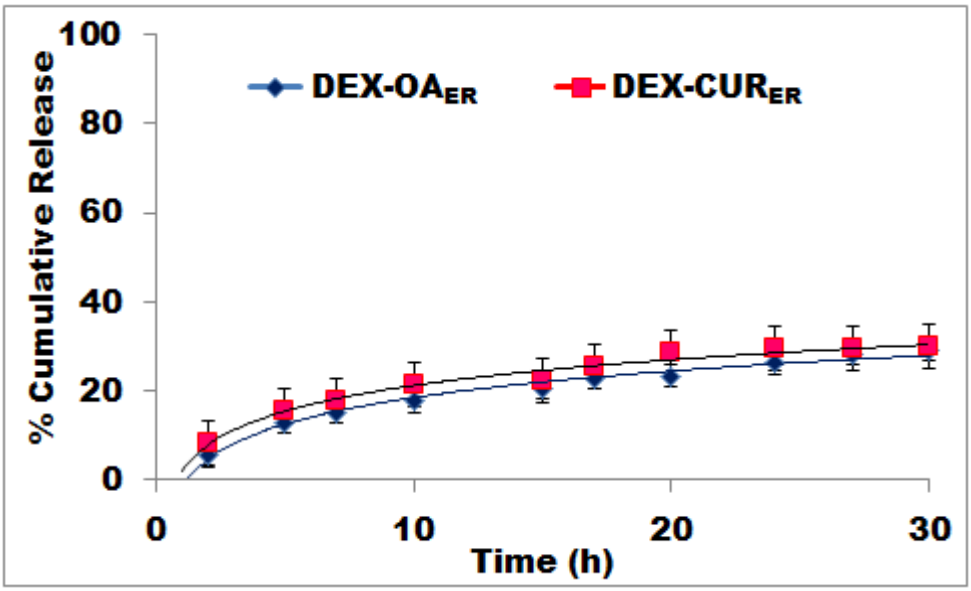

Figure 4.12: Cumulative release profile of DOX.HCl from both the carriers in FBS at 37 °C.

The degradation of these drug-loaded nanocarriers were also studied post its incubation in FBS using DLS **(Figure 4.13)**. The size of the vesicles and tubes remain intact even after 48 h of incubation corroborating with the phenomenon of minimal drug release.

4.3.5 Preclinical evaluation of the efficacy of nanoarchitectures for stimuli responsive anticancer therapy

The in-vivo performance of spherical nanocarriers with their non-spherical counterparts have been compared which has helped researchers to drawn conclusion that non-spherical carriers have demonstrated superior performance [51–53]. Further literature reports are suggestive of an effective endocytosis of nanotubes, nanowires and nano-filaments that are micrometer sized in length, particularly filomicelles having length ~8 µm have demonstrated effective cellular uptake [52]. It is noteworthy that designing long nanocarriers is an effective way to increase its blood circulation time of carriers. This ensures protection from liver and spleen clearance [35], [54]. The curcumin derived tubular carriers designed in this work corroborates with these finding. The 1-1.5 µm long tubular nanoarchitecture exhibited enhanced needle like tumor penetration due to its elated morphology which provides a better probability of interacting with the cellular surface as

compared to the spherical vesicles **(figure 4.14A, i & ii)**. The increased surface area provides a possibility of greater interaction between the carrier and the cells via multivalent ionic interactions resulting into an enhanced clathrin, caveolar mediated endocytosis [55]. This theory has been proved via cellular internalization experiments performed on MCF-7 cell lines. The calcein encapsulated nanoarchitectures are dosed to the cell lines and their internalization was monitored via fluorescence microscopic imaging.

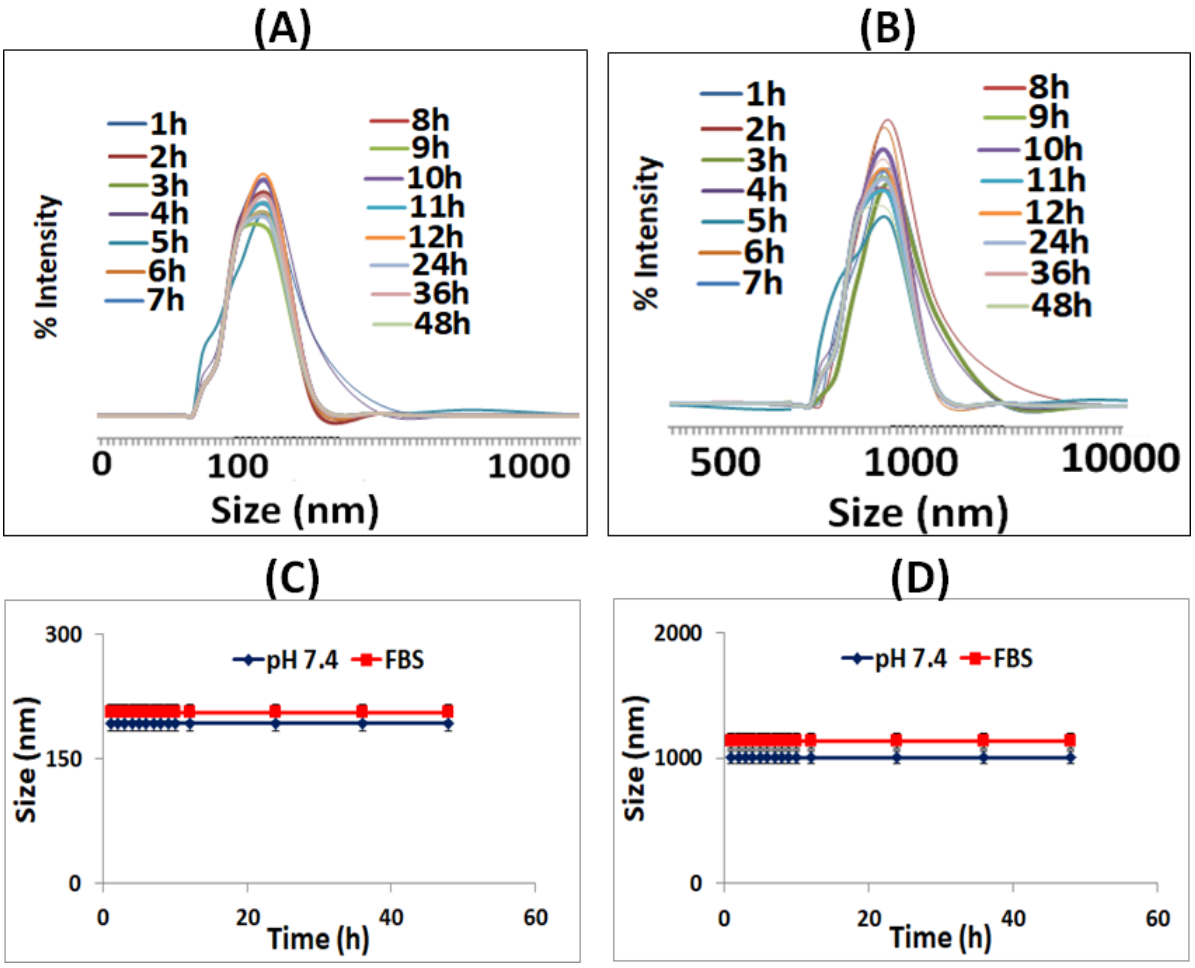

Figure 4.13: DLS plots showing size distribution of DOX.HCl loaded (A) DEX-OA_{ER} and (B) DEX-CUR_{ER} in FBS at 37 °C with respect to incubation time; Time versus size plot of DOX.HCl loaded (A) DEX-OA_{ER} and (B) DEX-CUR_{ER} in FBS at 37 °C.

The cell lines dosed only with calcein were considered as the control system, a punctuated fluorescence is an indicative of the endosomal/lysosomal encapsulation of the dye molecules in case of dye delivery in the absence of a carrier **(figure 4.15A).**

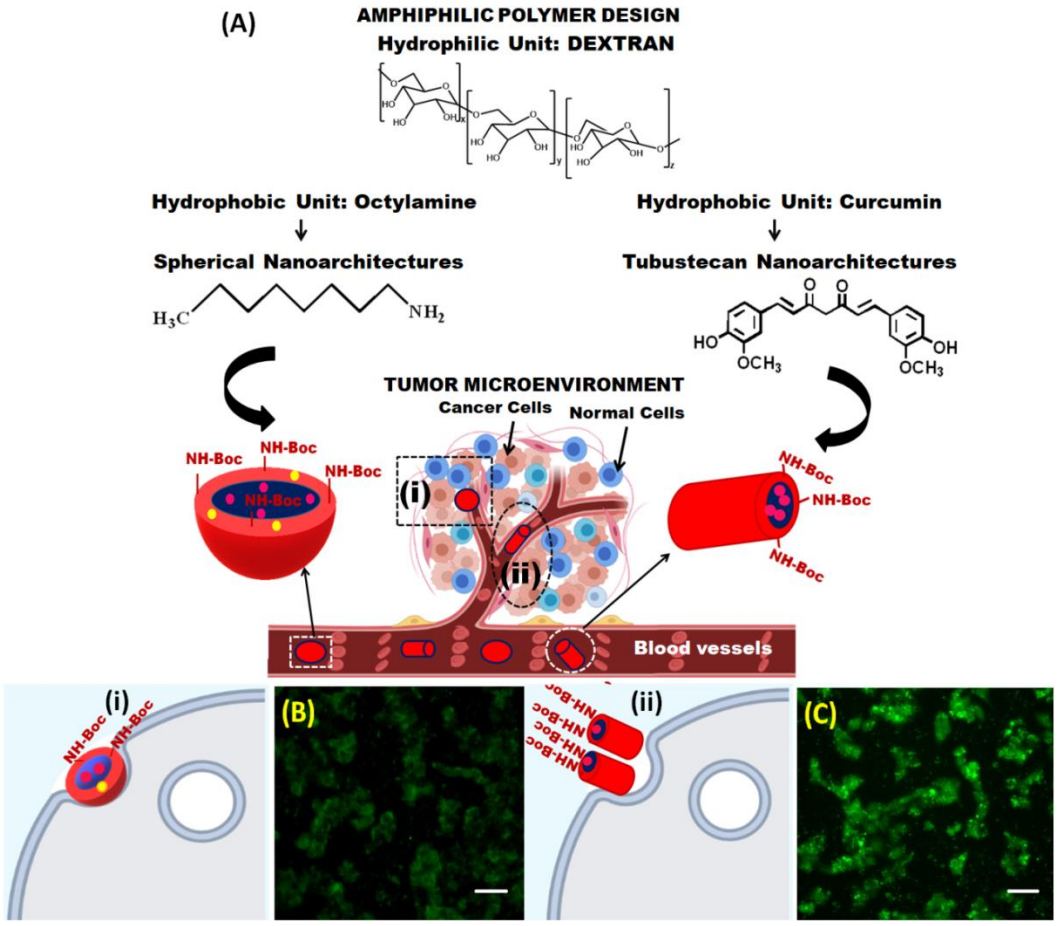

Figure 4.14: Schematic representation depicting (A) difference in morphologies of the nanoarchitectures upon change in the hydrophobic unit and (i), (ii) their cellular internalization; (B), (C) fluorescence microscopy images of calcein encapsulated nanoarchitectures internalized in MCF-7 cell lines (Scale 100 µm).

However, on the other hand when the dye molecules are escorted via entrapment in a carrier they are capable of exhibiting an endosomal escape and a uniform diffused fluorescence is emitted throughout the cells as observed in **figure 4.14 B & C** [56].

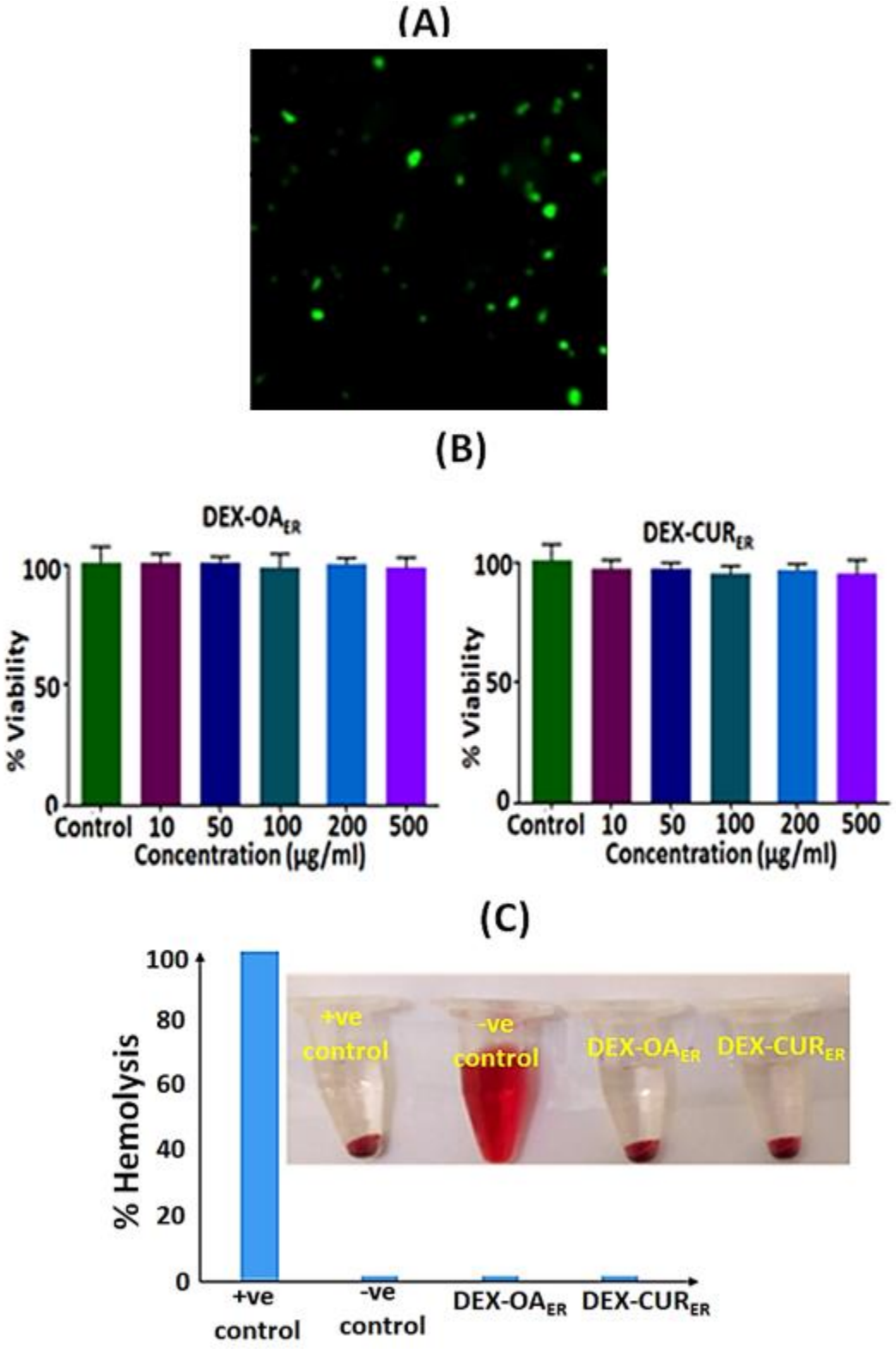

Figure 4.15: (A) Fluorescence microscopy image of bare calcein dosed to MCF-7 cells (B) MTT assay graphs and (C) Hemocompatibility of the carriers as per hemolysis assay

After an effective endocytosis and an early endosomal escape the carriers are encapsulated in the late endosomes wherein upon fusion with the lysosomes the carriers undergo an enzymatic cleavage under the influence of lysosomal enzymes [57]. This causes the release of some amount of drug from the carriers, in addition to this post the enzymatic action these carriers acquire their pH responsive form. Within the acidic intracellular environment the amine groups undergo protonation causing the polymer chains to swell and causing a leakage of rest of the drug molecules from the carriers [56] (as represented in **figure 4.16**).

Based on the tumor microenvironment modulation ability of both these nanoarchitectures, their efficacy as drug delivery vehicles were investigated via cytotoxicity and cellular uptake studies. For in-vitro studies human breast cancer cell lines were selected, the standard MTT assay indicated no significant toxicity towards the cell lines when they were dosed with only the carriers **(Figure 4.15 B)**, even upto dosage as high as 500 μg/ml**.** Although curcumin is the constituent of the carrier, it does not induce any toxicity because it is covalently bonded with dextran via stable urethane linkage. On the other hand, upon loading DOX.HCl in the carriers, its IC50 value decreases to 0.25 μg/ml from 0.5 μg/ml. Thus enabling the DOX.HCl loaded carriers to cause significant cell death at lower concentrations **(figure 4.17 B).** The tubular carrier showed more cellular inhibition as compared to its spherical counterpart. Moreover these injectable formulations were found to be hemocompatible as assessed from hemolysis assay **(figure 4.15 C)**. The PI staining studies provide corroborative evidences to the MTT assay. The released DOX molecules owing to their small size have the capability to enter the nucleus and undergo intercalation with DNA thus causing its damage and apoptotic cell death **(Figure 4.17 C).**

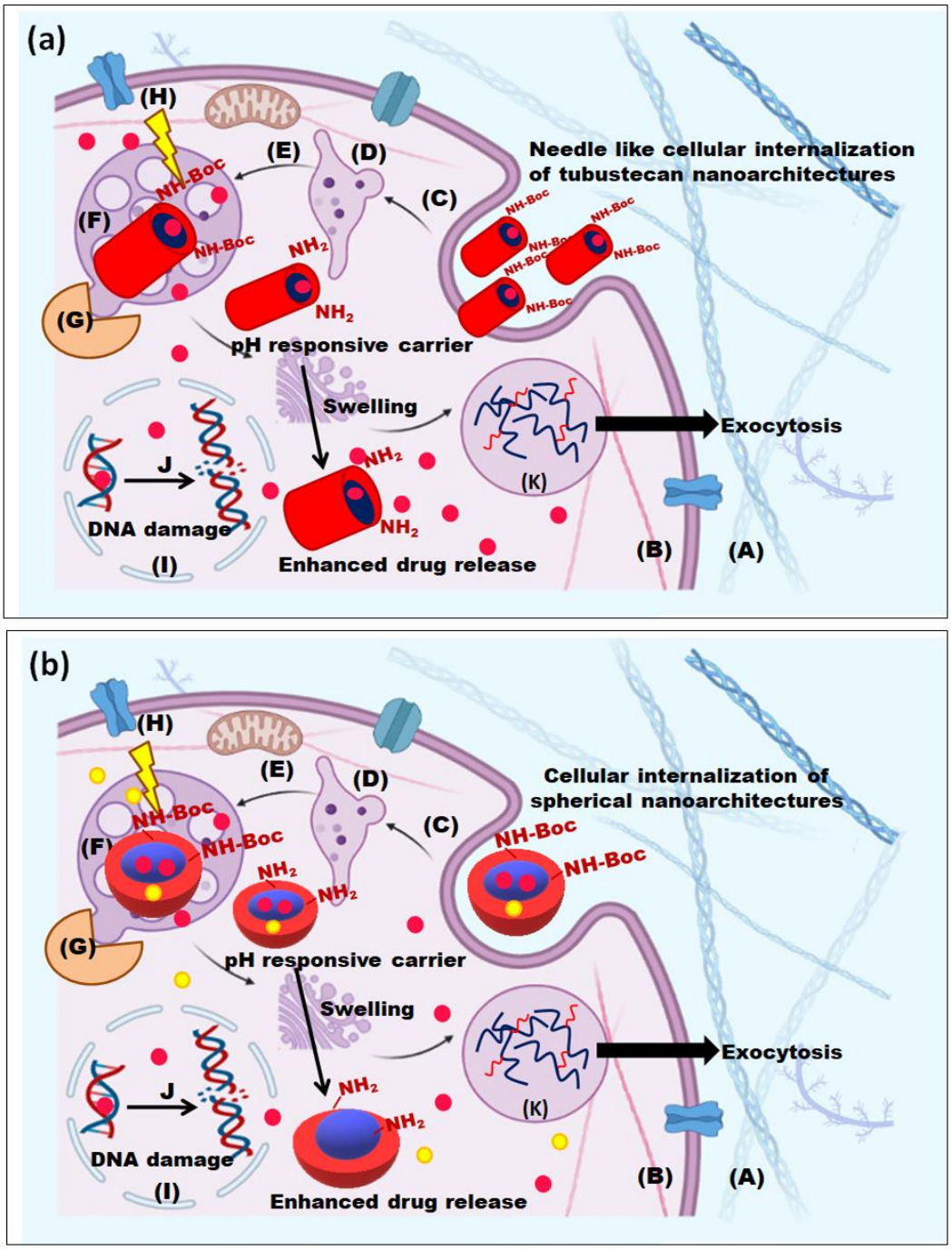

Figure 4.16: Probable mechanism of action of the drug release from the nanoarchitectures in the cellular environment.

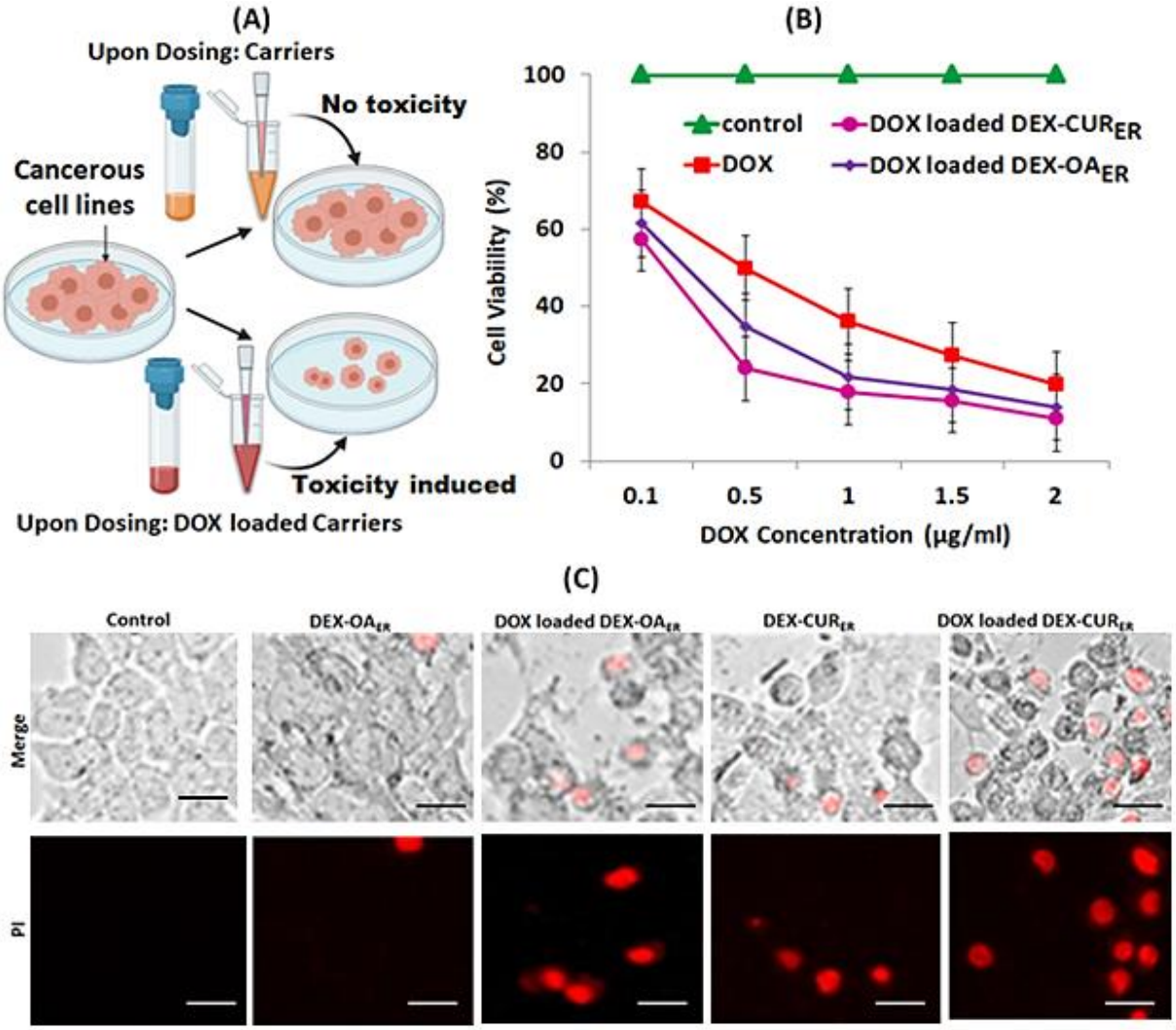

Figure 4.17: (A) Schematic representation of cell viabilities in presence of nanocarriers and drug loaded nanocarriers (B) MTT assay graphs (C) cell viability studies via PI staining technique (Scale 100 µm)

Post the in-vitro, studies the formulations were subjected to in-vivo evaluation. The animals were divided in various treatment groups as follows: the experiment consisted of 7 groups of animals with n=6 mice per group. The animals in group 1(G1) were dosed only with double distilled water and it was considered as control group. Various physiological parameters determined in this group were considered as the standard values for tumor free condition. The animals in the remaining groups (G2 to G7) were administered intraperitoneal injections of HEPG2 cells for the induction of hepatic tumor (HCC). Post successful tumor induction the animals of group 2 (G2)

were dosed with only PBS and this was considered as untreated group. The treatment groups comprised of group 3 (G3) dosed only with DOX.HCl group 4 (G4) dosed with DEX-CUR_{ER}, group 5 (G5) injected with DEX-OA_{ER}, group 6 (G6) administered with DOX.HCl loaded DEX-CUR_{ER} (10 mg kg^{-1}) and group 7 (G7) treated with DOX.HCl loaded DEX-$OA_{ER.}$

The schematic in **figure 4.18A** gives an overview of the treatment regimen. **Figure 4.18B** shows a drastic decrease in the body weight of G2 mice as compared to G1 following cancer development. The animals in groups G3 was dosed only with DOX.HCl. Groups G4 and G5 were treated only with nanocarriers (without drug). These groups showed weights similar to G2 mice which indicated that the nanocarriers do not influence the tumor growth. On the other hand, animals in G6 and G7 that are dosed with DOX.HCl loaded nanocarriers show a remarkable weight reduction (compared to untreated G2) and attain a weight similar to mice in control G1. Similar observations were noted when the liver weights **(figure 4.18C)** and liver indices (SGOT, SGPT) **(figure 4.19 A&B)** were studied. The analysis of matrix metallopeptidase (MMP) concentration in blood serum further demonstrated the effectiveness of the nanoarchitectures for a confined drug release at tumor site [58].

The MMPs are known to be up-regulated during all stages of cancer expression and metastasis and hence the efficacy of a drug delivery system can be related to their decreasing concentration post treatment.

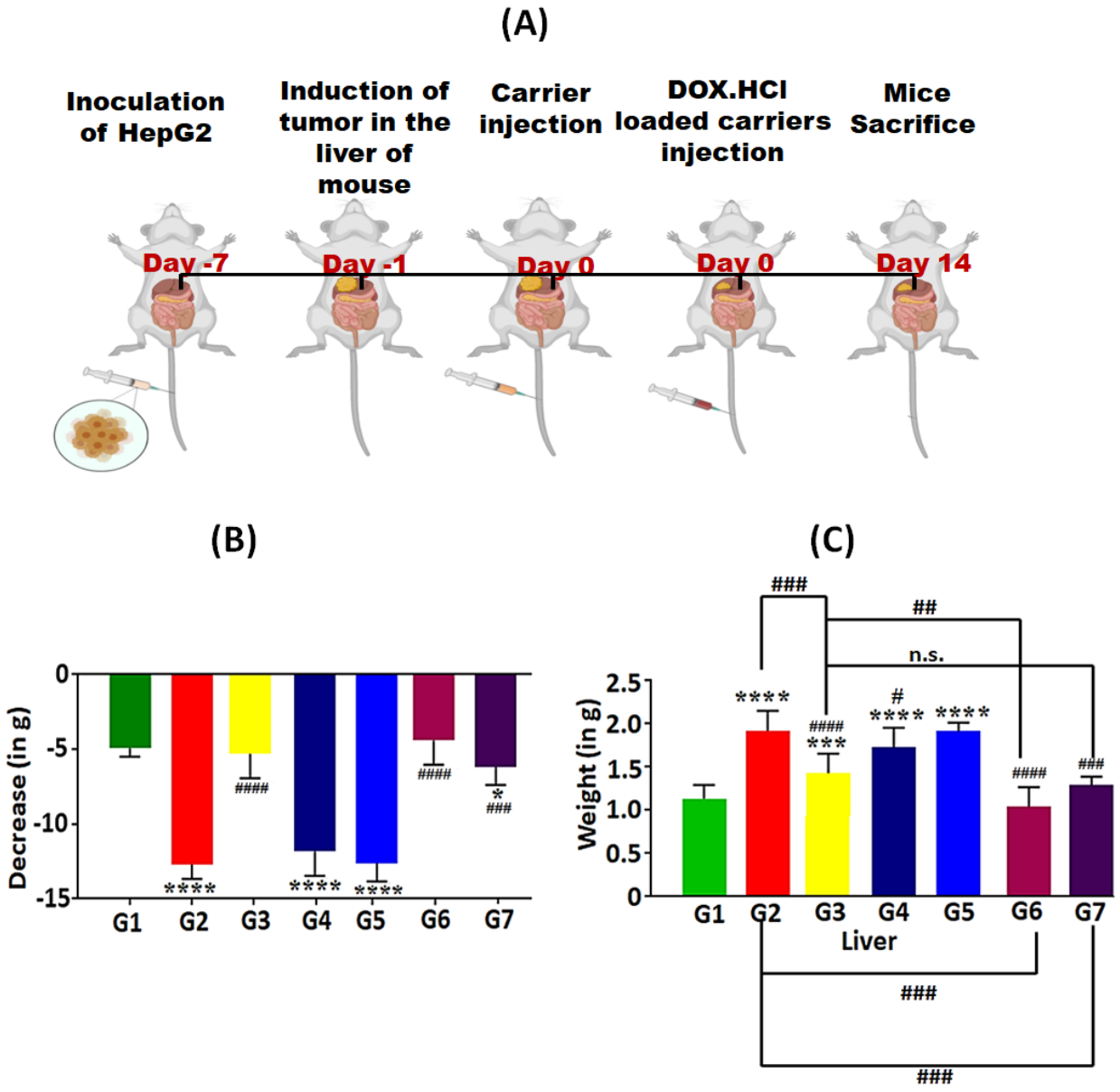

Figure 4.18: In-vivo studies performed on nude mice to establish the efficacy of carriers (A) schematic representation of the procedure; changes of (B) body weight (C) liver weight

The levels of MMP-2 and MMP-9 were analyzed in all the treatment groups as they are the biomarkers associated with invasiveness and metastasis of cancer **(figure 4.19 C & D)**. Very low levels of both the MMPs in G1 are an indicative of no cancer progression. On the contrary G2 shows highly elevated levels of MMP-2 and MMP-9, >400 ng/ml and >1000 ng/ml concentration respectively. Upon treatment with DOX.HCl loaded **DEX-CUR$_{ER}$** the graphs

show a drastic drop in concentration of both these proteins as compared to the DOX.HCL loaded **DEX-OA$_{ER}$** treatment. This confirms the role of an enhanced cellular internalization of tubular nanoarchitecture of **DEX-CUR$_{ER}$**. Similar observations were obtained when a glycoprotein biomarker specific to hepatocellular carcinoma named α-fetoprotein (AFP) was quantitatively measured following the treatment regimen [58]. A remarkably low concentration of AFP in the blood serum of animals in G6 and G7 as observed in **figure 4.19E** corroborate with the response of the mice towards treatment with drug loaded carriers.

The histoarchitechture of the liver tissue was also analyzed by hematoxylin and eosin staining of tumor tissue in all the groups is demonstrated in **figure 4.20A**. The histological stained liver of the mice in G2 predominantly showed tumor infiltration evident from severe mitoses and pleomorphic nuclei that are observed in the staining. However post treatment with drug loaded nanoarchitectures the tissues showed necrosis areas that are stained by eosin [55].

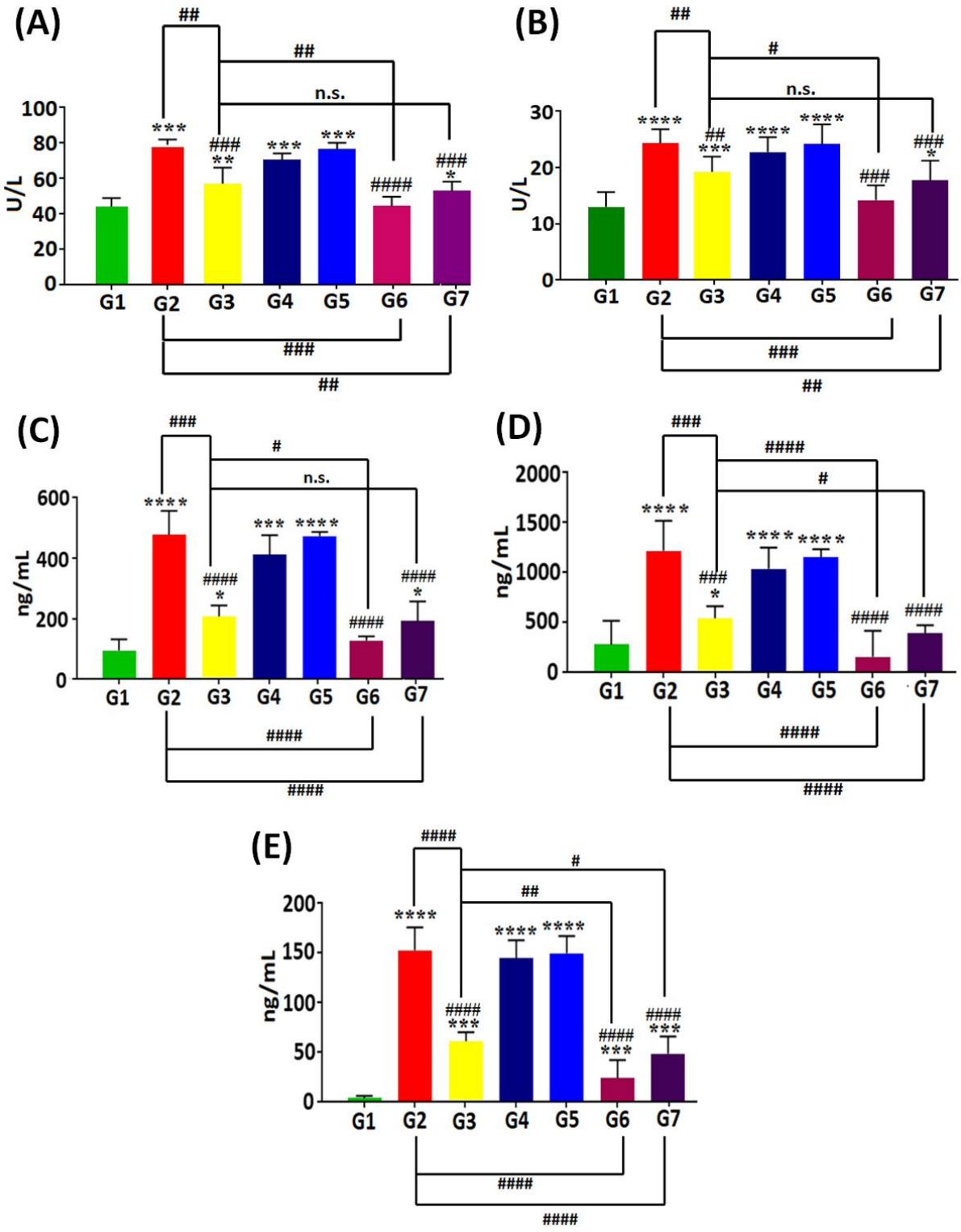

Figure 4.19: Quantitative assessment of liver indices viz (A) SGOT (B) SGPT in response to various treatments levels of (C) MMP-2, (D) MMP-9 and (E) AFP in blood serum.

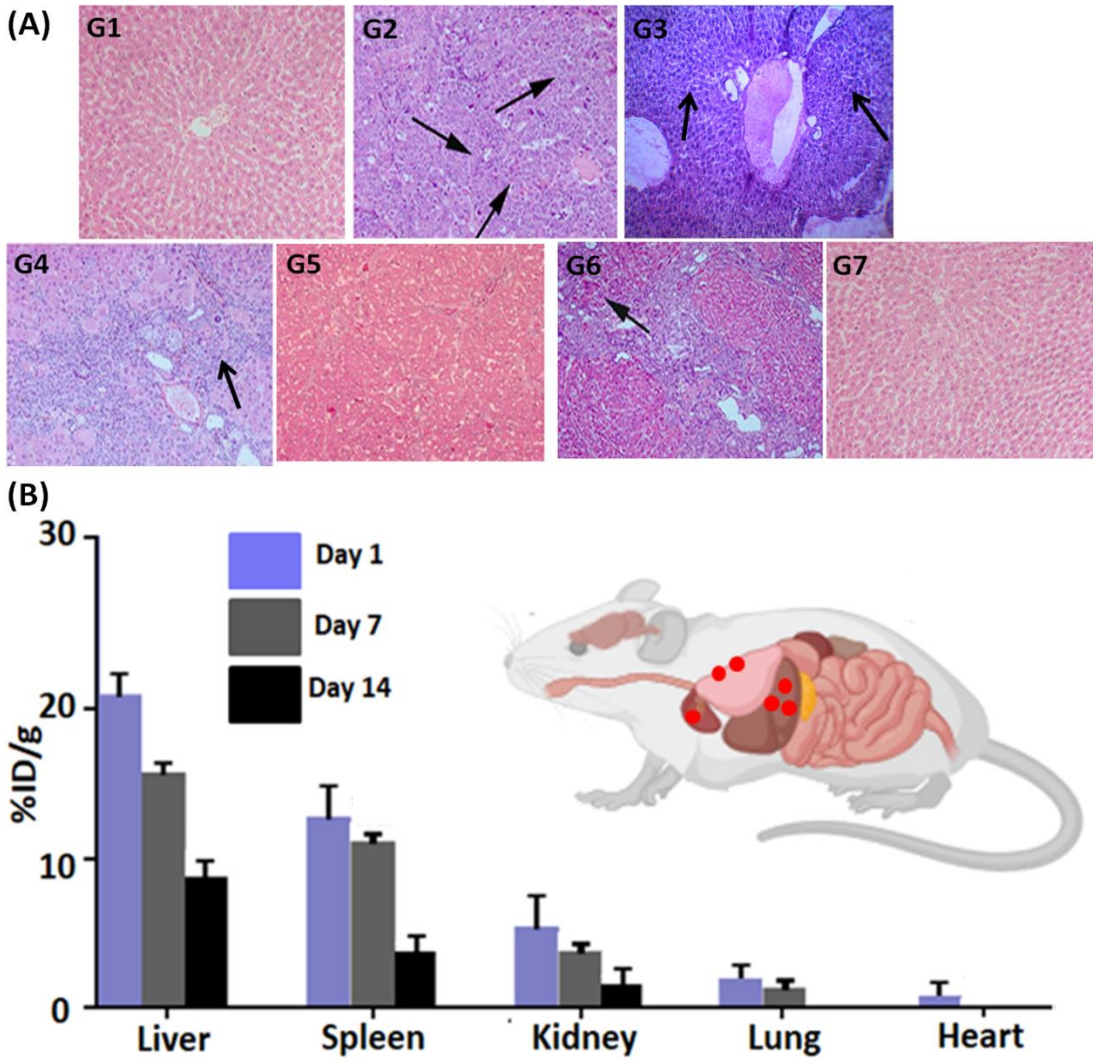

Figure 4.20 (A) H&E stained liver sections (Scale: 10 µm, 40X magnification) (C) Biosafety evaluation depicting clearance and accumulation of DOX.HCl in various organs during the treatment regimen.

From the study of all the above in-vivo parameters it was observed that, G6 mice treated with DOX.HCl loaded curcumin weaved tubular nanoarchitectures showed maximum tumor regression and least cardiotoxicity. This is owing to high drug loading capacity of the carriers coupled with its better internalization resulting into enhanced tumor homing. As discussed earlier DOX.HCl is considered as red devil owing to its high cardiotoxicity and thus when drug is administered as such, numerous side effects occur. This is owing to the bio-distribution of

DOX.HCl molecules into other healthy tissues. In the present work, the entrapment of DOX.HCl molecules into the nanoarchitectures assisted in overcoming its acute toxicity. This is evident from the observations that there is nearly no damage or inflammation of other organs like heart, lungs, kidney and spleen of the tumor bearing mice dosed with the nanoarchitectures **(figure 4.21 A-E and 4.22)**.

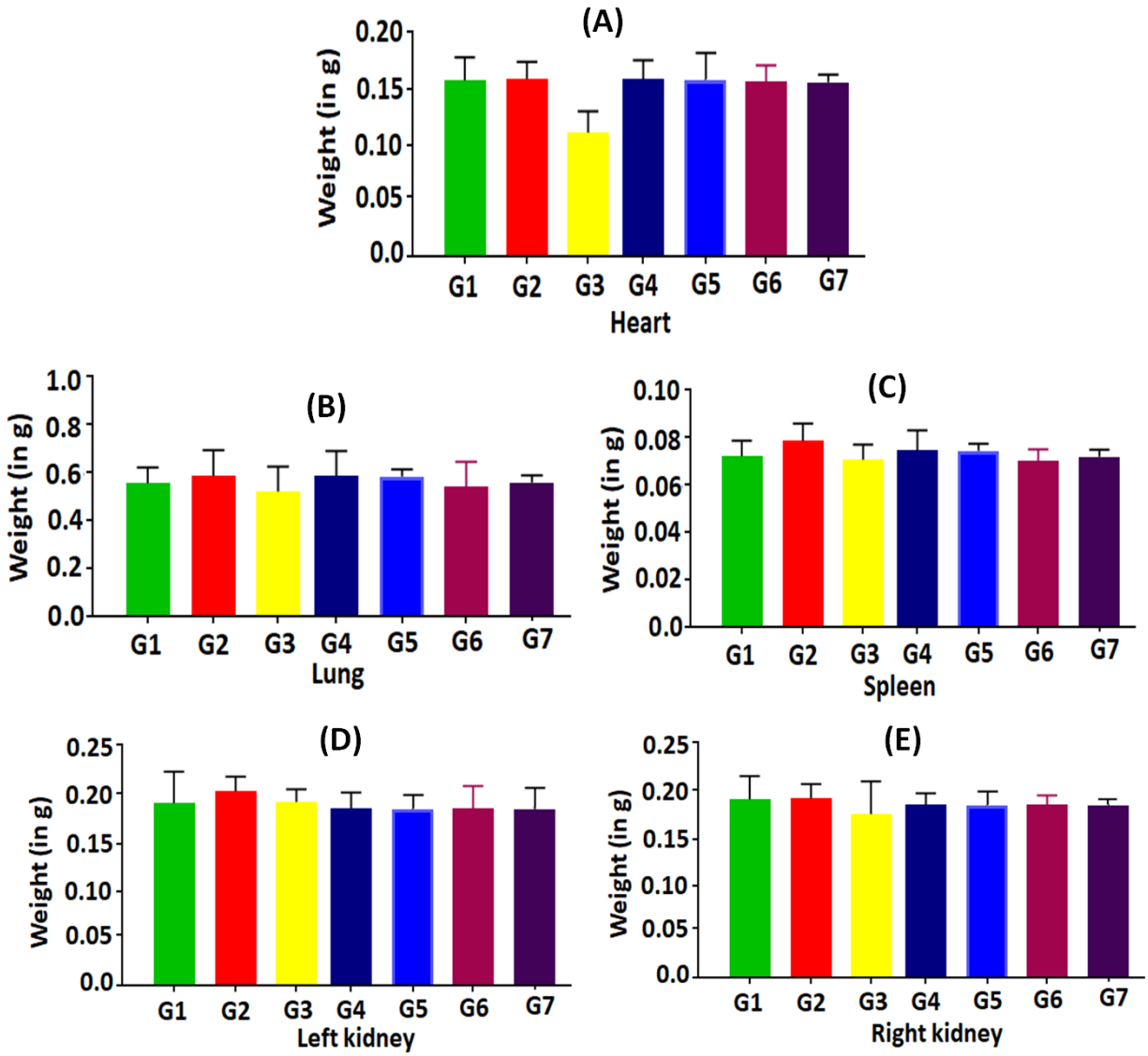

Figure 4.21: Analysis of the effect of treatment on weight of (A) Heart (B) Lung (C) spleen (D) Right kidney (E) Left kidney.

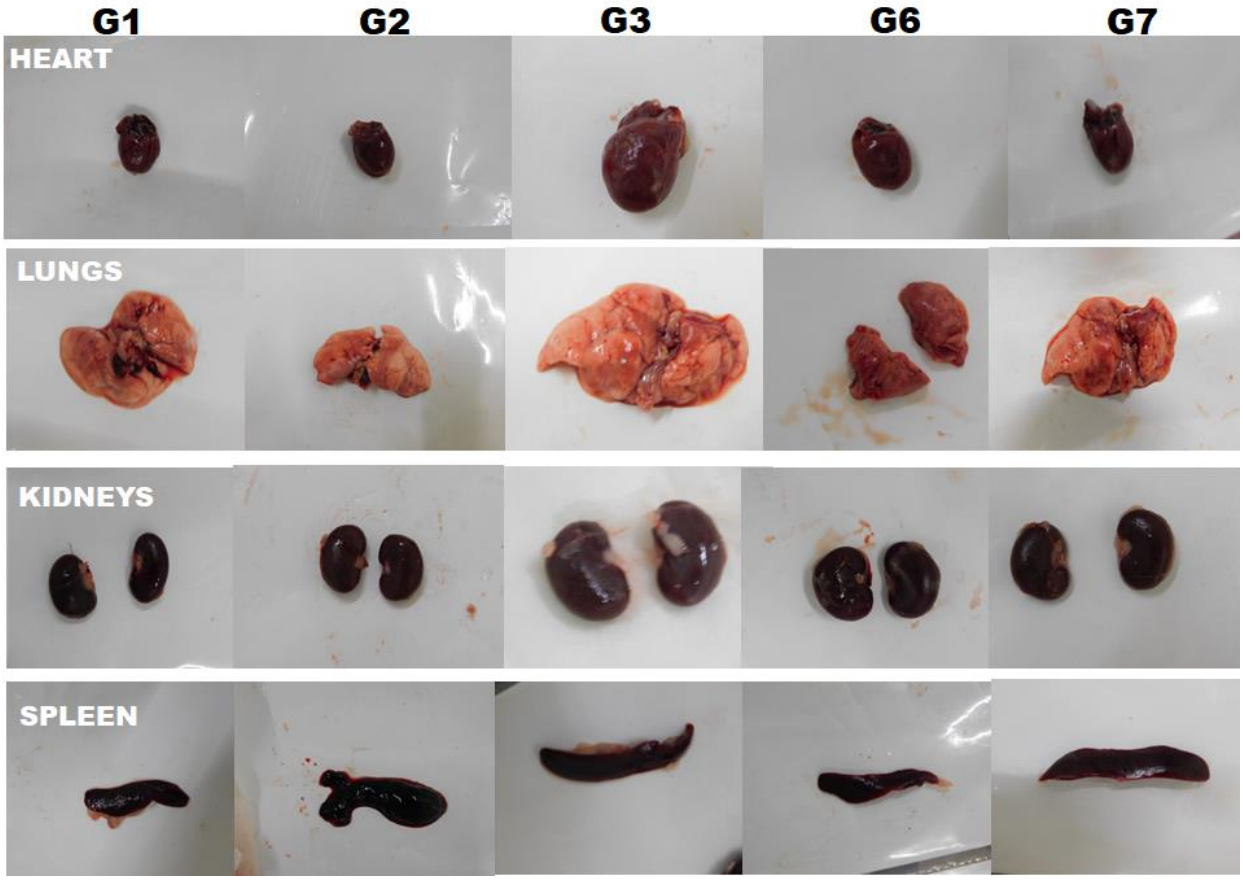

Figure 4.22: Images of various organs demonstrating reduced toxicity of DOX.HCl upon delivery via tubular nanoarchitectures

Moreover, it is noteworthy that majority of the nanocarriers injected into the animals are cleared from their systems post 14 days of injection **(figure 4.20 B)**. It was also observed that majority of the carrier accumulation occurs into the liver which is the site of tumor some percentage into the spleen which is indicative of hepatic clearance in the process of excretion. These results indicate the biocompatibility and biosafety of the nanoarchitectures as drug carriers for efficacious cancer therapy.

4.4 Conclusion

This work is thus an attempt to develop dextran derived amphiphiles using two different hydrophobic components that self-assemble into different morphologies. Using curcumin as a hydrophobic component of the amphiphile self-assembled into tubular nanoarchitectures with

small mouth aperture of 20 nm and length ~1 μm. On the other hand, using octylamine as hydrophobic component the amphiphile self-assembled into spherical vesicles of 190 nm. The tubular and spherical nanoassemblies demonstrated 55% and 50 % entrapment efficiency for DOX. It was observed that although the vesicles hold a good potential of delivering both hydrophilic and hydrophobic drugs, they were comparatively less efficient than the tubustecan nanoarchitectures. This was an attribute of the shape of the carriers. The nanotubes showed the efficacy to undergo internalization while escaping the endosomal degradation. This prevents the drug leakage prior to reaching the tumor site. The nanoarchitectures released the encapsulated drug only upon the trigger of tumor microenvironment i.e. pH and enzyme thus ensuring a cancer cell specific delivery. The tubular nanocarriers demonstrated more drug loading capability due to its shape as well as a sustained drug release upto 30 h. The drug release occurred in presence of esterase (enzyme) and upto 35 h in the intracellular pH. The superlative performance of tubular system was confirmed from drug loading potential, cumulative release profiles, cellular internalization experiment and various in-vivo parameters. This also led to reduced cardiotoxicity of notorious DOX as observed in the biological clearance studies in-vivo. Thus such biogenic system can be effectively used to control the severe toxicity of well-known drugs presenting an avenue to reposition the existing drug for efficacious chemotherapy.

4.5 References

1. Parhizkar M, Reardon PJT, Harker AH, Browning RJ, Stride E, Pedley RB, Knowles JC, Edirisinghe M. 2020: 1177–1186.
2. Lyu YL, Ã LFL. In *Recent Advances in Cancer Research and Therapy* 2012; pp 351–169.
3. Farokhzad OC, Langer R. *ACS Nano*. 2009; 3: 16–20.
4. Kumar R, Dalvi S V., Siril PF. Nanoparticle-Based Drugs and Formulations: Current Status and Emerging Applications, 2020, vol. 3.
5. Tavakkoli Yaraki M, Pan Y, Hu F, Yu Y, Liu B, Tan YN. *Mater Chem Front*. 2020; 4: 3074–3085.
6. Sahoo AK, Goswami U, Dutta D, Banerjee S, Chattopadhyay A, Ghosh SS. *ACS Biomater Sci Eng*. 2016; 2: 1395–1402.
7. He X, Peng C, Qiang S, Xiong LH, Zhao Z, Wang Z, Kwok RTK, Lam JWY, Ma N, Tang BZ. *Biomaterials*. 2020; 238: 119834.

8. Wang Q, Zhang X, Sun Y, Wang L, Ding L, Zhu WH, Di W, Duan YR. *Biomaterials*. 2019; 212: 73–86.
9. Cai Z, Zhang Y, He Z, Jiang LP, Zhu JJ. *ACS Appl Bio Mater*. 2020; 3: 5322–5330.
10. Adokoh CK, Keter FK, Kinfe HH, Tshikhudo R, Darkwa J. *RSC Med Chem*. 2020; 11: 283–292.
11. Das M, Solanki A, Joshi A, Devkar R, Seshadri S, Thakore S. *Carbohydr Polym*. 2019; 206: 694–705.
12. Solanki A, Sanghvi S, Devkar R, Thakore S. *RSC Adv*. 2016; 6: 98693–98707.
13. Lassenberger A, Scheberl A, Batchu KC, Cristiglio V, Grillo I, Hermida-Merino D, Reimhult E, Baccile N. *ACS Appl Bio Mater*. 2019; 2: 3095–3107.
14. Ding X, Yu W, Wan Y, Yang M, Hua C, Peng N, Liu Y. *Carbohydr Polym*. 2020; 245: 116493.
15. Paula D, Lucena-s E, Escudero A, Llopis-lorente A, Villalonga R. 2021.
16. Ong C, Cha BG, Kim J. *ACS Appl Bio Mater*. 2019; 2: 3630–3638.
17. Das M, Nariya P, Joshi A, Vohra A, Devkar R. *Carbohydr Polym*. 2020; 247: 116751.
18. Hong G, Diao S, Antaris AL, Dai H. *Chem Rev*. 2015; 115: 10816–10906.
19. Wu F, Su H, Cai Y, Wong W, Jiang W, Zhu X. 2018.
20. Iannazzo D, Ziccarelli I, Pistone A. *J Mater Chem B*. 2017; 5: 6471–6489.
21. Shao L, Zhang R, Lu J, Zhao C, Deng X, Wu Y. *ACS Appl Mater Interfaces*. 2017; 9: 1226–1236.
22. Mallick A, Nandi A, Basu S. *ACS Appl Bio Mater*. 2019; 2: 14–19.
23. Managa M, Ngoy BP, Nyokong T. *New J Chem*. 2019; 43: 4518–4524.
24. Nan X, Zhang X, Liu Y, Zhou M, Chen X, Zhang X. *ACS Appl Mater Interfaces*. 2017; 9: 9986–9995.
25. Jain P, Patel K, Jangid AK, Guleria A, Patel S, Pooja D, Kulhari H. *ACS Appl Bio Mater*. 2020; 3: 6852–6864.
26. Tang J, Li B, Howard CB, Mahler SM, Thurecht KJ, Wu Y, Huang L, Xu ZP. *Biomaterials*. 2019; 216: 119232.
27. Wang CF, Sarparanta MP, Mäkilä EM, Hyvönen MLK, Laakkonen PM, Salonen JJ, Hirvonen JT, Airaksinen AJ, Santos HA. *Biomaterials*. 2015; 48: 108–118.
28. Luk B, Zhang L. *ACS Appl Mater Interfaces*. 2014; 6: 21859–21873.

29. Ravichandran G, Rengan AK. *ACS Appl Nano Mater*. 2020; 3: 9542–9559.
30. Wang F, Hu S, Sun Q, Fei Q, Ma C, Lu C, Nie J, Chen Z, Ren J, Chen GR, Yang G, He XP, James TD. *ACS Appl Bio Mater*. 2019; 2: 4904–4910.
31. Guleria M, Sharma R, Amirdhanayagam J, Sarma HD, Rangarajan V, Dash A, Das T. *RSC Med Chem*. 2021; 12: 263–277.
32. Yang X, Grailer JJ, Rowland IJ, Javadi A, Hurley SA, Steeber DA, Gong S. *Biomaterials*. 2010; 31: 9065–9073.
33. Caracciolo G, Palchetti S, Digiacomo L, Chiozzi RZ, Capriotti AL, Amenitsch H, Tentori PM, Palmieri V, Papi M, Cardarelli F, Pozzi D, Laganà A. *ACS Appl Mater Interfaces*. 2018; 10: 22951–22962.
34. Shroff K, Kokkoli E. *Langmuir*. 2012; 28: 4729–4736.
35. Mane SR, Sathyan A, Shunmugam R. *ACS Appl Nano Mater*. 2020; 3: 2104–21117.
36. Wang J, Wang F, Li F, Zhang W, Shen Y, Zhou D, Guo S. *J Mater Chem B*. 2016; 4: 2954–2962.
37. Ou X, Zheng J, Zhao X, Liu M. *ACS Appl Nano Mater*. 2018; 1: 6790–6799.
38. Mizushina Y, Ishidoh T, Takeuchi T, Shimazaki N, Koiwai O, Kuramochi K, Kobayashi S, Sugawara F, Sakaguchi K, Yoshida H. *Biochem Biophys Res Commun*. 2005; 337: 1288–1295.
39. Deshpande NU, Jayakannan M. *Biomacromolecules*. 2017; 18: 113–126.
40. Mondal T, Dan K, Deb J, Jana SS, Ghosh S. *Langmuir*. 2013; 29: 6746–6753.
41. Nanoparticles PW. *Langmuir*. 2017; 33: 5275–5282.
42. Sagle LB, Zhang Y, Litosh VA, Chen X, Cho Y, Cremer PS. *J Am Chem Soc*. 2009; 131: 9304–9310.
43. Aluri R, Jayakannan M. *Biomacromolecules*. 2017; 18: 189–200.
44. Feng G, Mao D, Liu J, Goh CC, Ng LG, Kong D, Tang BZ, Liu B. *Nanoscale*. 2018; 10: 5869–5874.
45. Le Fer G, Portes D, Goudounet G, Guigner JM, Garanger E, Lecommandoux S. *Org Biomol Chem*. 2017; 15: 10095–10104.
46. Yan G, Wang J, Hu L, Wang X, Yang G, Fu S, Cheng X, Zhang P. *Acta Biomater*. 2017; 51: 363–373.
47. Hao G, Xu ZP, Li L. *RSC Adv*. 2018; 8: 22182–22192.

48. Neri D, Supuran CT. *Nat Rev Drug Discov*. 2011; 10: 767–777.
49. Park JH, Von Maltzahn G, Zhang L, Derfus AM, Simberg D, Harris TJ, Ruoslahti E, Bhatia SN, Sailor MJ. *Small*. 2009; 5: 694–700.
50. Venkataraman S, Hedrick JL, Yuin Z, Yang C, Lai P, Ee R, Hammond PT, Yan Y. *Adv Drug Deliv Rev*. 2011; 63: 1228–1246.
51. Geng Y, Dalhaimer P, Cai S, Tsai R, Tewari M, Minko T, Discher DE. *Nat Nanotechnol*. 2007; 2: 249–255.
52. Christian DA, Cai S, Garbuzenko OB, Harada T, Zajac AL, Minko T, Discher DE. *Mol Pharm*. 2009; 6: 1343–1352.
53. Fernando D, Sulthana S, Vasquez Y. *ACS Appl Bio Mater*. 2020; 3: 1374–1384.
54. Dey SK, Dan K, Das MR, Saha S, Das P, Ghosh S, Jana SS. *Biomater Sci*. 2013; 1: 1211–1215.
55. Chithrani BD, Ghazani AA, Chan WCW. *Nano Lett*. 2006; 6: 662–668.
56. Wong ASM, Mann SK, Czuba E, Sahut A, Liu H, Suekama C, Bickerton T, Johnston PR, Such GK. *Soft Matter*. 2015; 11: 2993–3002.
57. Kashyap S, Singh N, Surnar B, Jayakannan M. *Biomacromolecules*. 2015; 17: 384–398.
58. Isaacson KJ, Jensen MM, Subrahmanyam NB, City SL, Chemistry P, City SL, City SL. *J Control Release*. 2018; 10: 62–75.